

Pacific Northwest National Laboratory

Operated by Battelle for the
U.S. Department of Energy

Electrically Switched Cesium Ion Exchange

FY 1997 Annual Report

Michael A. Lilga
Rick J. Orth
Johanes P.H. Sukamto
Scot D. Rassat
David Genders
Ram Gopal

RECEIVED
DEC 18 1997
OSTI

September 1997

Prepared for the U.S. Department of Energy
under Contract DE-AC06-76RLO 1830

DISCLAIMER

This report was prepared as an account of work sponsored by an agency of the United States Government. Neither the United States Government nor any agency thereof, nor Battelle Memorial Institute, nor any of their employees, makes any warranty, express or implied, or assumes any legal liability or responsibility for the accuracy, completeness, or usefulness of any information, apparatus, product, or process disclosed, or represents that its use would not infringe privately owned rights. Reference herein to any specific commercial product, process, or service by trade name, trademark, manufacturer, or otherwise does not necessarily constitute or imply its endorsement, recommendation, or favoring by the United States Government or any agency thereof, or Battelle Memorial Institute. The views and opinions of authors expressed herein do not necessarily state or reflect those of the United States Government or any agency thereof.

PACIFIC NORTHWEST NATIONAL LABORATORY

operated by

BATTELLE

for the

UNITED STATES DEPARTMENT OF ENERGY

under Contract DE-AC06-76RLO 1830

Printed in the United States of America

Available to DOE and DOE contractors from the
Office of Scientific and Technical Information, P.O. Box 62, Oak Ridge, TN 37831;
prices available from (615) 576-8401.

Available to the public from the National Technical Information Service,
U.S. Department of Commerce, 5285 Port Royal Rd., Springfield, VA 22161



This document was printed on recycled paper.

Electrically Switched Cesium Ion Exchange

FY 1997 Annual Report

Michael A. Lilga
Rick J. Orth
Johanes P. H. Sukamto
Scot D. Rassat
Pacific Northwest National Laboratory

David Genders
Ram Gopal
The Electrosynthesis Company, Inc.

September 1997

DISTRIBUTION OF THIS DOCUMENT IS UNLIMITED *ph*

MASTER

Prepared for
the Office of Science and Technology
U.S. Department of Energy Office of Environmental Management
Efficient Separations and Processing Crosscutting Program
under Contract DE-AC06-76RLO 1830

Pacific Northwest National Laboratory
Richland, Washington 99352

DISCLAIMER

Portions of this document may be illegible electronic image products. Images are produced from the best available original document.

Summary

Electrically Switched Ion Exchange (ESIX) is a separation technology being developed at Pacific Northwest National Laboratory (PNNL) as an alternative to conventional ion exchange for removing radionuclides from high-level waste. In conventional ion exchange, secondary wastes are generated with each step needed to complete the removal process (acid elution, exchanger water rinse, and sodium loading of the exchanger). Other disadvantages include a high sodium content of the waste, which affects the waste form for disposal, and frequent replacement of exchangers. The ESIX technology, which combines ion exchange and electrochemistry, is geared toward producing electroactive films that are highly selective, regenerable, and long lasting. During the process, ion uptake and elution can be controlled directly by modulating the potential of an ion exchange film that has been electrochemically deposited onto a high surface area electrode. This method adds little sodium to the waste stream and minimizes the secondary wastes associated with traditional ion exchange techniques.

Development of the ESIX process is well underway for cesium removal using ferrocyanides as the electroactive films. Films having selectivity for perrhenate (a pertechnetate surrogate) over nitrate also have been deposited and tested at PNNL. Based on the ferrocyanide film capacity, stability, rate of uptake, and selectivity shown during performance testing, it appears possible to retain a consistent rate of removal and elute cesium into the same elution solution over several load/unload cycles. In batch experiments during FY 1997, metal hexacyanoferrate films showed high selectivities for cesium in concentrated sodium solutions. In these experiments, cesium uptake was unaffected by Na/Cs molar ratios of up to 2×10^4 , and reached equilibrium within 18 hours. During engineering design tests using 60 pores per inch, high surface area nickel electrodes, nickel ferrocyanide films displayed continued durability, losing less than 20% of their capacity after 1500 load/unload cycles. Bench-scale flow system studies showed no change in capacity or performance of the ESIX films at a flow rate up to 113 BV/h, the maximum flow rate tested, and breakthrough curves further supported once-through waste processing.

Two types of electrochemical cells, and flow patterns, were evaluated during FY 1997: a Micro Flow cell in flow-through mode (work conducted by PNNL) and an MP cell in flow-by mode (work conducted under subcontract by The Electrosynthesis Co., Inc.). Comparison of results for a stacked 5-electrode cell versus a single electrode cell in the flow-through configuration showed enhanced breakthrough performance. In the stacked configuration, breakthrough began at about 120 BV for a feed containing 0.2 ppm cesium at a flow rate of 13 BV/h. Also, performance in single electrode flow-by mode was better than in single electrode flow-through mode.

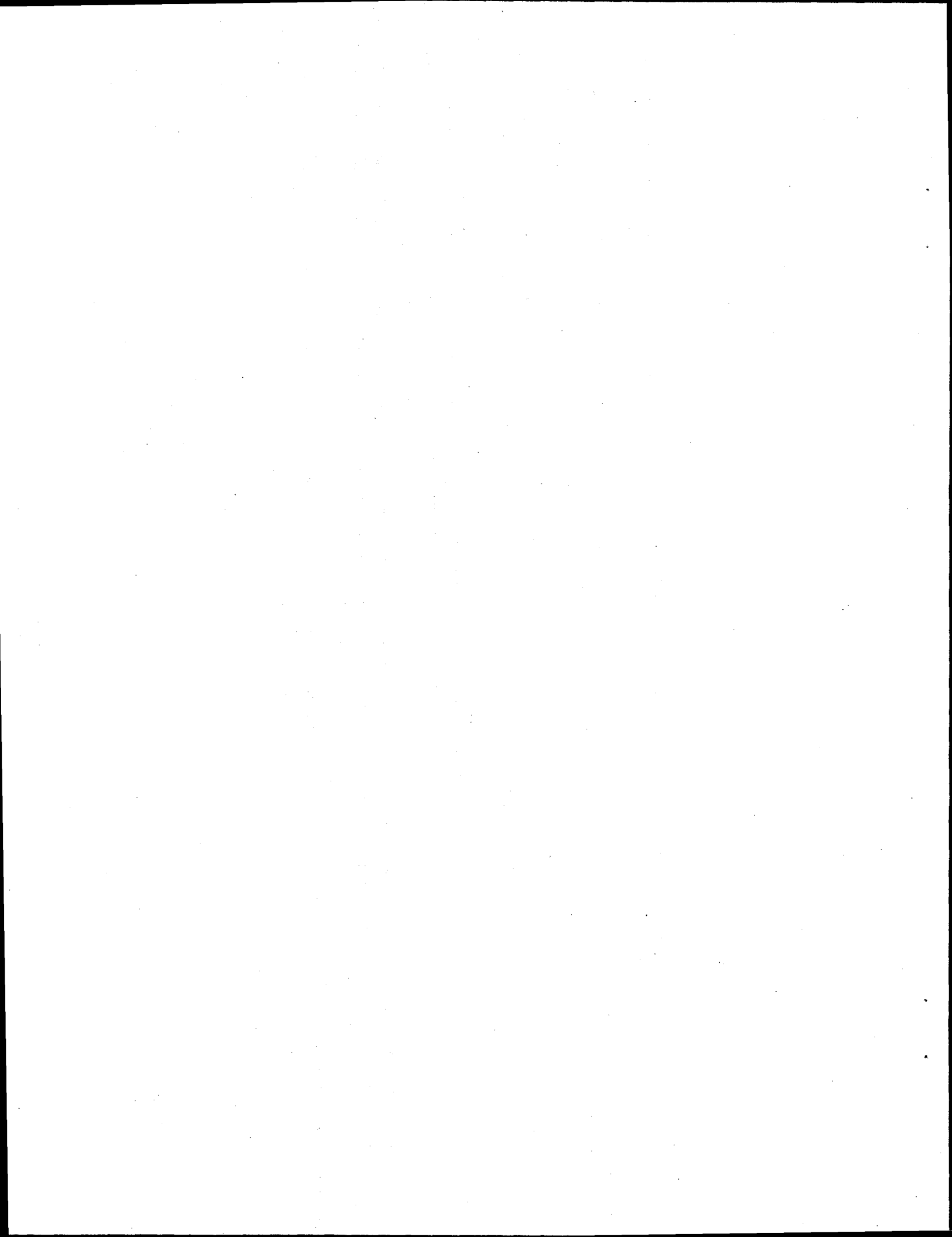
A case study for the KE Basin on the Hanford Site was conducted based on the results of the experimental testing and modeling efforts. Engineering design baseline parameters for film deposition, film regeneration, cesium loading, and cesium elution were used for developing a

conceptual system. Order of magnitude cost estimates were developed to compare with conventional ion exchange. This case study demonstrated that KE Basin wastewater could be processed continuously with minimal secondary waste and reduced associated disposal costs, as well as lower capital and labor expenditures.

Work planned for the ESIX technology in FY 1998 includes further optimization of the process with waste simulants. Demonstrating the process with actual wastes will depend on funding availability.

Acknowledgments

This work was funded by the Office of Science and Technology within the Department of Energy's Office of Environmental Management and under the Efficient Separations and Processing Crosscutting Program. LDRD funding was received for developing the ESIX technology for other applications.



Contents

Summary	iii
Acknowledgments	v
1.0 Introduction	1.1
1.1 Technology Description.....	1.2
1.2 Advantages of ESIX	1.2
1.3 Target Applications.....	1.3
1.4 Summary of Results of Previous Studies	1.3
2.0 Work Accomplished.....	2.1
2.1 Experimental	2.1
2.2 Batch Results.....	2.5
2.3 Flow Cell Results	2.8
2.3.1 Micro Flow Cell Results Using a Single Electrode	2.8
2.3.2 Micro Flow Cell Results Using Stacked Electrodes.....	2.11
2.3.3 MP Results Using a Single Electrode	2.13
2.4 Modeling of Micro Flow Cell and MP Cell Data	2.16
2.5 ESIX Case Study for KE Basin Application.....	2.20
2.5.1 Bases and Assumptions	2.20
2.5.2 Process Concept and Estimated Costs.....	2.23
2.5.3 Potential Advantages of ESIX for KE Basin Application.....	2.24
3.0 Conclusions	3.1
4.0 References	4.1
Appendix A Development of ESIX Films Selective for Per technetate	
Appendix B Contractor Report. Electrochemically Switched Ion Exchange	

Figures

1. The ESIX Concept for Cesium Ion Loading and Unloading	1.2
2. Solution Flow Patterns in Electrochemical Cells Used for Flow Tests	2.1
3. Micro Flow Cell Apparatus with a Single Electrode	2.2
4. Close-up of the Micro Flow Cell with a Single Electrode	2.2
5. Micro Flow Cell Apparatus with 5-electrode Stack	2.3
6. Close-up of the Micro Flow Cell with 5-electrode Stack	2.3
7. MP Cell Experimental Setup	2.4
8. Effect of Applied Potential on Cesium Uptake in Batch Experiments	2.7
9. Effect of Sodium on Cesium Uptake in Batch Experiments	2.7
10. Effect of Elution Solution on Cesium Unloading in Batch Experiments	2.8
11. Effect of Flow Rate on Cesium Breakthrough in Flow-through Mode	2.9
12. Effect of $[Cs]_0$ on Cesium Breakthrough in Flow-through Mode	2.10
13. Consistency of Performance for Two Separate Electrodes in Flow-through Mode	2.11
14. Effect of Flow Rate on Cesium Breakthrough in a Micro Flow Cell Containing Five Stacked Electrodes Operated in Flow-through Mode	2.12
15. Effect of Feed Cesium Concentration on Cesium Breakthrough in an MP Cell Containing a Single Electrode Operated in Flow-by Mode	2.13
16. Model Fit to Breakthrough Data for $[Cs]_0 = 0.2$ ppm and Flow Rate = 13, 37, and 113 BV/h in Flow-through Mode for Five Stacked Electrodes	2.18
17. Model Fit to Breakthrough Data for $[Cs]_0 = 0.2$ ppm and Flow Rate = 13, 37, and 113 BV/h in Flow-through Mode for Five Stacked Electrodes. Model Calculated for $\kappa a \propto v^{0.39}$	2.18
18. Model Fit to Breakthrough Data for $[Cs]_0 = 0.2$ ppm and Flow Rate = 13, 37, and 113 BV/h in Flow-through Mode for Five Stacked Electrodes. Model Calculated for $\kappa a \propto v^{0.61}$	2.19

19. Model Fit to Breakthrough Data for $[Cs]_0 = 0.2$ ppm and Flow Rate = 13, 37, and 113 BV/h in Flow-through Mode for Five Stacked Electrodes. Model Calculated for $\kappa a \propto v^{0.7}$	2.19
20. Model Fit to Breakthrough Data for Flow Rate = 8.5 BV/h and $[Cs]_0 =$ 0.18, 1.03, and 1.35 ppm and in Flow-by Mode for a Single Electrode	2.20
21. Model Fit to Breakthrough Data for $[Cs]_0 = 0.2$ ppm and Flow Rate = 13 BV/h in Flow-through Mode for Single and Stacked Electrodes.....	2.21
22. Predicted Breakthrough for ESIX Treatment of KE Basin Water at 13 BV/h for feeds of 10^{-7} and 10^{-10} M Cs	2.21
23. Flow Diagram for Waste Decontamination with ESIX	2.22
24. Conceptual Schematic Electrode Arrangement for KE Basin Decontamination.....	2.23

Tables

1. Actual and Theoretical Cesium Loading on 60 ppi Nickel Foam Electrodes.....	2.6
2. Summary of Results from Micro Flow Cell Tests.....	2.10
3. Performance of 60 ppi Nickel Foam Electrodes in Flow-by Mode as a Function of Feed Cesium Concentration.....	2.14
4. Reproducibility and Flow Rate Dependence of Nickel Foam Electrodes in Flow-by Mode.....	2.15

1.0 Introduction

Radioactive wastes throughout the various U.S. Department of Energy (DOE) sites comprise many forms, including fuel storage basin water; underground storage tanks containing high-level radioactive waste (HLW); and groundwater. Along with safety and regulatory requirements for the final waste form, economic considerations, such as the high cost of vitrifying HLW, compel the removal of radionuclides before the procedures for permanent disposal can be carried out. Separating out and concentrating most of the radionuclides would allow the bulk of the waste to be disposed of less expensively as low-level waste (LLW).

The needed separations are not easy, as illustrated by the requirements for radioactive cesium (^{137}Cs). Based on the concentration of ^{137}Cs in tank waste (about 10^{-4} M) and the required level of decontamination, the separation process must have a decontamination factor of at least 5500. The separation must also be selective for cesium in the presence of sodium concentrations that can be 10^5 times higher. Radioactive cesium concentrations in spent nuclear fuel storage basins (10^{-10} M) and groundwater (10^{-13} M) are much lower than those found in tank waste, but the concentrations of sodium and potassium are still several orders of magnitude higher than cesium. A method of removing cesium is needed that avoids transuranic (TRU) loading of the waste form and does not generate large quantities of secondary waste.

The most accepted option for cesium separation before final disposal is conventional ion exchange. Both inorganic and organic ion exchangers are under consideration. Unfortunately, for regenerable ion exchange materials, a large amount of secondary waste results from the numerous process steps required (acid elution, exchanger water rinse, and sodium loading of the exchanger). Neutralization of the acidic eluant typically adds sodium to the waste, restricting the choice of waste form and limiting the amount of waste that can be incorporated. In addition, it has been reported that organic exchangers lose approximately 3% of their capacity per cycle (Kurath et al. 1994). Therefore, typical organic exchangers can be used for only 20 to 30 cycles before they must also be disposed of as another form of secondary waste. Most inorganic ion exchange materials are not regenerable, adding substantial costs for ion exchange replacement and secondary waste disposal. The technology discussed in this report is being developed to provide a more economical remediation alternative.

Electrically Switched Ion Exchange (ESIX), being developed at Pacific Northwest National Laboratory (PNNL),^(a) combines ion exchange and electrochemistry to provide a selective, reversible method for radionuclide separation that lowers costs typically associated with conventional ion exchange and minimizes secondary waste generation. The ESIX technology is described here, along with progress in FY 1997 for specific applications.

^(a) Operated for the U.S. Department of Energy by Battelle under Contract DE-AC06-76RLO 1830.

1.1 Technology Description

In the ESIX process, an electroactive ion exchange film is deposited onto a high surface area electrode, and ion uptake and elution are controlled directly by modulating the potential of the film. At PNNL, films for cesium removal have been prepared and tested, and process development and optimization are well underway. For cesium, the electroactive films being tested are ferrocyanides, which are well known to have high selectivities for cesium in concentrated sodium solutions. When a cathodic potential is applied to the film, Fe^{+3} is reduced to the Fe^{+2} state, and a cation must be intercalated into the film to maintain charge neutrality (i.e., Cs^+ is loaded). Conversely, if an anodic potential is applied, a cation must be released from the film (i.e., Cs^+ is unloaded). Therefore, to load the film with cesium, the film is simply reduced; to unload cesium, the film is oxidized. Figure 1 illustrates the concept for cesium.

In further work at PNNL, a different proprietary film selective for ReO_4^- (a pertechnetate surrogate) has also been developed (see Appendix A). In ReO_4^- (i.e., TcO_4^-) separation, loading occurs when the film is oxidized and unloading occurs upon film reduction.

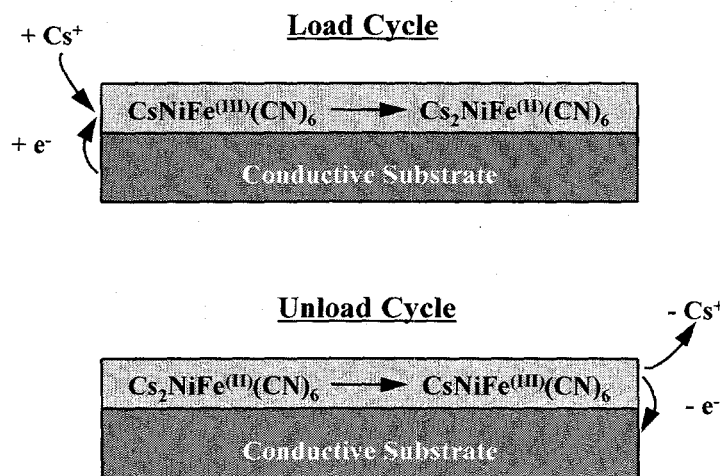


Figure 1. The ESIX Concept for Cesium Ion Loading and Unloading

1.2 Advantages of ESIX

ESIX is a regenerable ion exchange process that has great potential to minimize secondary waste and produce a low-sodium, cesium-rich waste stream. An important advantage of the ESIX process is that cesium can be eluted into the same elution solution over several load cycles, because the unload step is conducted electrochemically without added chemicals and is independent of the soluble cesium concentration. This improved process would result in the

generation of a waste stream with a very low sodium concentration and a cesium concentration that is limited only by solubility, radiation, and heat generation. Such a HLW feed stream allows for a broader range of final waste forms, including those that cannot tolerate sodium. The production of secondary waste would be minimized, since the large volumes of solution associated with elution, wash, and regeneration cycles typical of standard ion exchange are not needed for the ESIX process. A small amount of wash solution may be necessary after the unload cycle, but this solution could be used in subsequent cycles for unloading the exchanger. Ratios of the volume of generated secondary waste to the volume of processed waste are estimated to be as low as 0.0006 for the ESIX process, or about two orders of magnitude lower than for a typical regenerable process using commercially available CS-100 ion exchange resin.

1.3 Target Applications

Based on current ESIX process knowledge, the most likely applications of this technology for cesium separations are for waste streams with a pH less than about 11. Target wastes include basin water (KE Basin, KW Basin, and N Basin at the Hanford Site; Savannah River Site basins), basin sludge, groundwater (TAN TSF-05 Injection Well at the Idaho Site), offgas scrubber solutions from the vitrification process, and acidic tank wastes (Idaho Site). This technology could also find application for treatment of wastewater generated during decontamination and decommissioning operations and other waste processing activities across the DOE complex.

The recent development of films selective for ReO_4^- , a surrogate for radioactive TcO_4^- , shows promise for application of the ESIX technology to technetium-bearing wastes and groundwater.

1.4 Summary of Results of Previous Studies

The objective of the project discussed here is to establish the viability of ESIX by increasing the stability and capacity of electroactive films and determining uptake and elution parameters of the process under flow conditions. Work in FY 1996 to develop the ESIX technology for cesium separation focused on deposition of films with higher capacities and stabilities than for previously reported films (Bocarsly and Sinha 1982). The results from the FY 1996 testing were used for expanded testing in FY 1997 that included deposition on high surface area electrodes and bench-scale flow studies. A conceptual process was devised for cesium separation based on a case study of the Hanford KE Basin.

Deposition procedures were developed in FY 1996 (Lilga et al. 1996) for nickel ferrocyanide films, $\text{M}_2\text{NiFe}(\text{CN})_6$ ($\text{M} = \text{Na}, \text{K}$), on flat-plate or high surface area nickel foam electrodes. These films are prepared by electrochemically oxidizing the nickel electrode in a $\text{Fe}(\text{CN})_6^{3-}$ solution, precipitating the active film on the electrode surface. Electrochemical deposition gives reproducible films with reversible behavior; i.e., metal ions are loaded and unloaded reversibly by switching the electrode potential. Films prepared by modified literature

procedures (named PNNL-1 and -2) have higher capacity and stability than those previously reported in the literature, and retain the high selectivity for cesium that ferrocyanide materials are known to possess.

This durability is illustrated, for example, by films prepared to date on flat-plate electrodes, which have almost twice the capacity of previously reported films and lose less than 20% of their capacity after 2000 load/unload cycles. In contrast, a literature film on a flat plate lost 50% of its capacity after the same cycling. Furthermore, in studies during FY 1997, films on 60 pores per inch (ppi) ($40 \text{ cm}^2/\text{cm}^3$), high surface area nickel foam electrodes lost only about 20% of their capacity after 1500 load/unload cycles. Flow cell experiments showed that films on 60 ppi electrodes were stable at least up to 113 bed volumes per hour (BV/h), the maximum flow rate tested.

The use of metal hexacyanoferrates, which are known cesium ion exchange materials (Lehto and Harjula 1987), gives high selectivity for cesium over sodium as shown by cyclic voltammetry (Lilga et al. 1996) and in FY 1997 batch experiments. In the batch experiments, cesium uptake was unaffected by Na/Cs molar ratios of up to 2×10^4 . Cesium uptake reached equilibrium within 18 h in the batch experiments.

2.0 Work Accomplished

Research completed in FY 1997 entailed batch studies of cesium loading and unloading on high surface area nickel foam electrodes and on flow cell testing of hexacyanoferrate-coated electrodes for cesium separation. Details of the experimental procedures are reported in Section 2.1, and findings are discussed in Sections 2.2 and 2.3. Modeling (Section 2.4) and a case study (Section 2.5) were performed for KE Basin water at the Hanford Site to obtain a preliminary estimate of the required equipment size and capital costs.

2.1 Experimental

Flow cell tests were conducted in two types of electrochemical cells, a Teflon Micro Flow cell (ElectroCell AB) and an MP cell (ElectroCell AB). Each cell had a different flow pattern. The Micro Flow cell was used in PNNL tests in which solution passed through the face of a 2.8 x 2.1 x 0.64 cm ESIX electrode. This type of flow is called flow-through mode and, for the electrodes used, the bed depth was 0.64 cm (0.25") per electrode in the cell. Figure 2 illustrates the flow-through mode, as well as the flow-by mode discussed below. The performance of a single electrode (cell and experimental apparatus shown in Figures 3 and 4) and a stack of 5 electrodes in series (Figures 5 and 6) was tested in this cell. Before flow testing began, batch tests were conducted to study film capacity and regeneration.

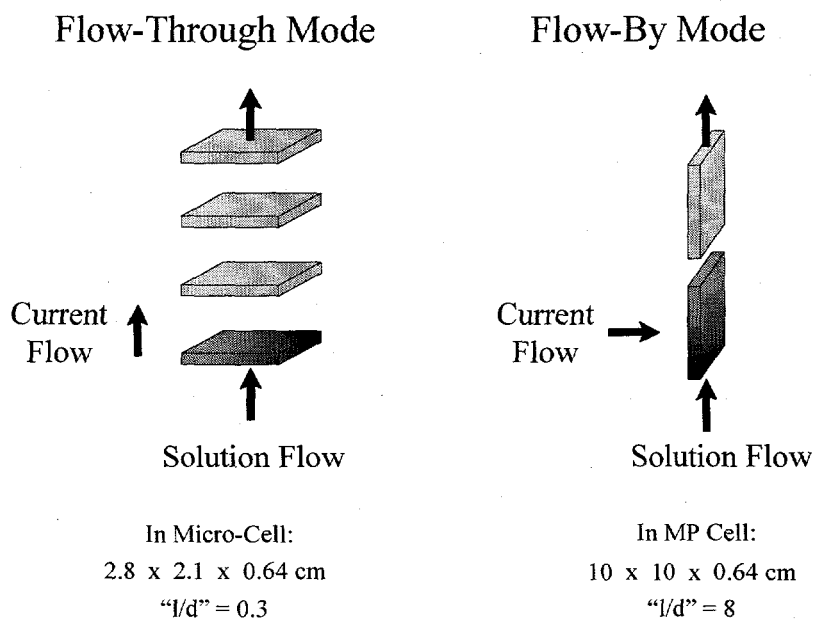


Figure 2. Solution Flow Patterns in Electrochemical Cells Used for Flow Tests

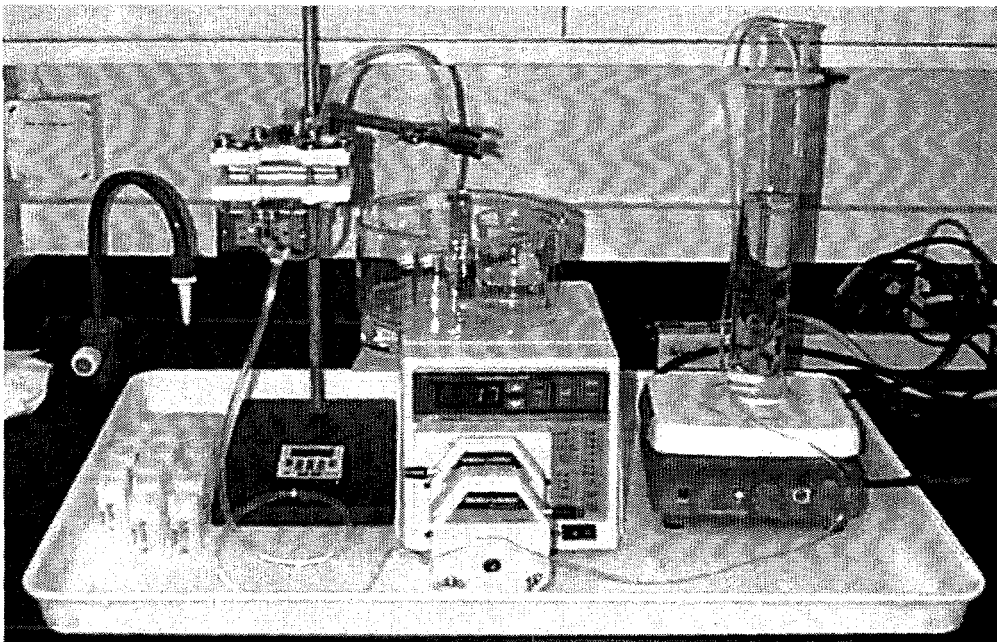


Figure 3. Micro Flow Cell Apparatus with a Single Electrode

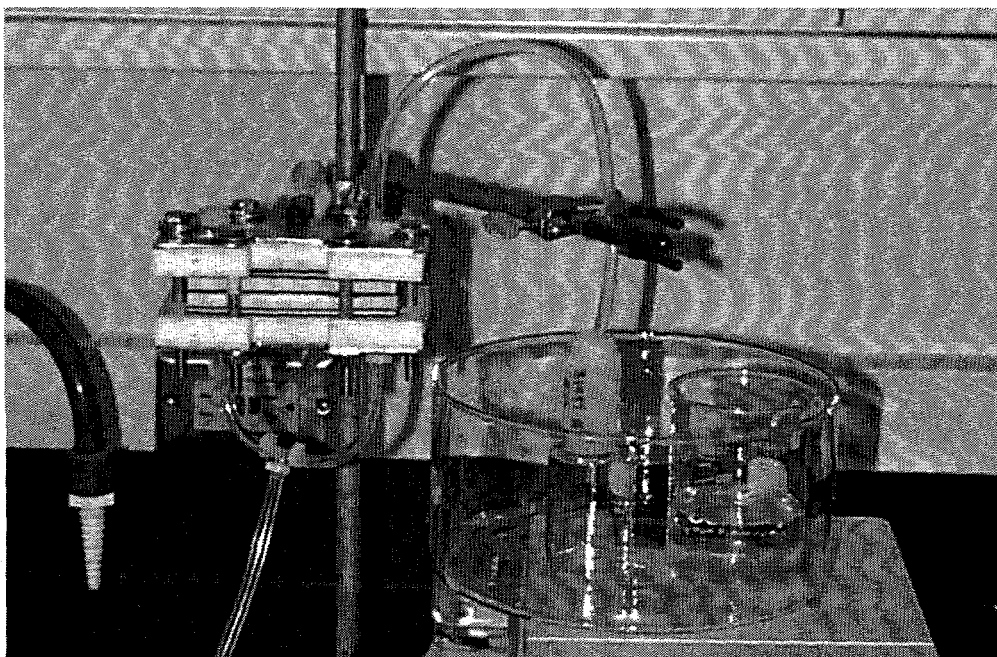


Figure 4. Close-up of the Micro Flow Cell with a Single Electrode

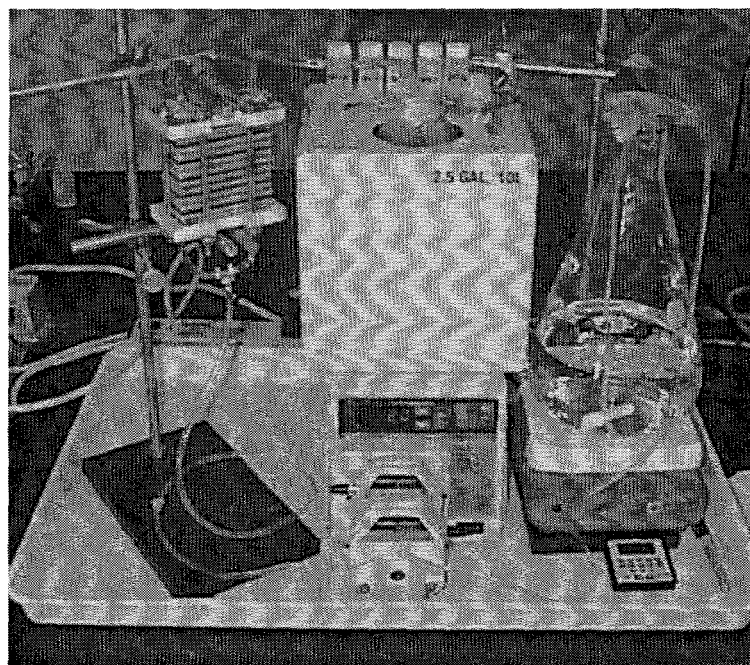


Figure 5. Micro Flow Cell Apparatus with 5-electrode Stack

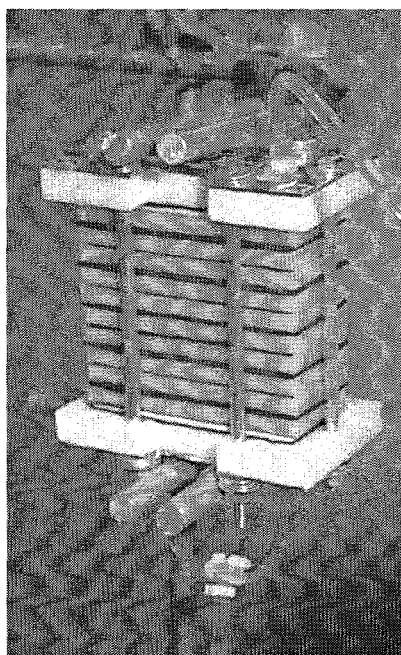


Figure 6. Close-up of the Micro Flow Cell with 5-electrode Stack

The MP cell was modified to house the nickel foam electrode (Figure 7). Solution flow in this cell (flow-by) passed through the length of a 10 cm x 10 cm x 0.64 cm electrode (bed depth of 10 cm). The Electrosynthesis Co., Inc., performed MP cell tests; their findings are summarized in Section 2.2.3 and reported in Appendix B.

In both cell designs, cesium ion exchange was conducted on open circuit; i.e., the cesium feed solution passed through regenerated electrodes without the application of an electrochemical potential or current. After a cesium ion exchange experiment, electrodes were regenerated either in situ or ex situ (after cell disassembly) by applying a controlled current or controlled potential, respectively. A Masterflex pump was used to control liquid flow through the cells at the desired rate (5 to 45 mL/min in Micro Flow cell tests; 8 to 24 mL/min in MP cell tests). Effluent samples were collected at predetermined intervals for cesium analysis. Cesium analyses were conducted by flame emission atomic absorption spectrophotometry. Samples were diluted with an aqueous potassium solution for increased sensitivity for cesium ion.

In PNNL testing, a PAR 273A potentiostat/galvanostat (Princeton Applied Research) was used to deposit and characterize films. Potentials were recorded versus a saturated calomel electrode (SCE). Experiments were controlled and data collected with a Dell 466/MX computer via a GPIB card using LabView™ software.

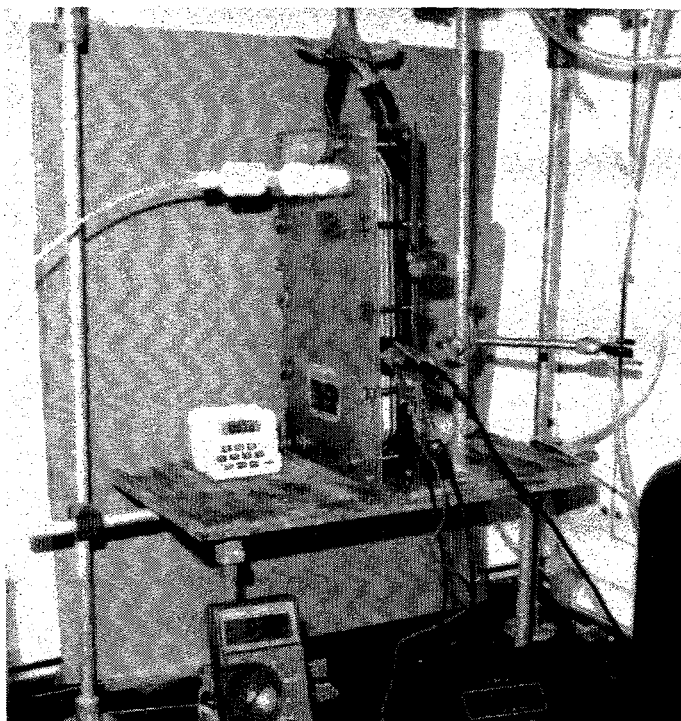


Figure 7. MP Cell Experimental Setup

Nickel foam electrodes (supplied by The Electrosynthesis Co., Inc.) with a nominal surface area per volume of $40 \text{ cm}^2/\text{cm}^3$ (60 ppi) coated with nickel hexacyanoferrate films were used in all PNNL batch and Micro Flow cell experiments. Films were deposited using a PNNL-proprietary method (PNNL-2) similar to that of Bocarsly and Sinha (1982), where the nickel surface was exposed to a solution of $5 \text{ mM K}_3\text{Fe}(\text{CN})_6$ and 0.1 M KNO_3 , and a 1.0 V (SCE) potential was applied to the nickel electrode for 300 s. All chemicals were A.C.S. reagent grade, and solutions were prepared with $18.2 \text{ M}\Omega\text{-cm}$ water.

Cyclic voltammetry and chronocoulometry were used to characterize and regenerate films. Cyclic voltammetry was typically conducted in 1 M NaNO_3 solutions starting from an applied potential of 0.25 V , scanning anodically to 0.8 V , then cathodically to -0.1 V , returning to 0.25 V (SCE) at a scan rate of 50 mV/s . Chronocoulometry was conducted by stepping to 0.25 V (SCE) to load the film and to 0.5 V (SCE) to unload the film, also in 1.0 M NaNO_3 .

In experiments conducted at The Electrosynthesis Co., Inc., porous nickel foams of porosity 60 and 80 ppi were used. The same PNNL method for film preparation was used except the electrolyte for film deposition was a solution containing 0.1 M KNO_3 and $10 \text{ mM K}_3\text{Fe}(\text{CN})_6$, and a PAR 273 potentiostat was used to control the potential. All voltammograms were done at a scan rate of 50 mV/s between -0.25 and $1.05 \text{ V vs. Ag/AgCl}$. The oxidation and reduction waves were integrated to obtain the film loading or capacity of the film. Chronocoulometric experiments were also performed to determine the film capacity. The areas under the current decay curves at 0.8 V and 0.2 V (potentials vs. Ag/AgCl) for 30 s each were used to measure film capacities.

Regeneration of films in situ involved passing a solution of 0.1 M NaNO_3 through the cell while maintaining a low constant current (5 mA). A low current was used in these initial tests to demonstrate the viability of the in situ method, but a higher current would give faster regeneration. Passage of about 300 mL of 0.1 M NaNO_3 solution for about 2 to 3 h was sufficient to elute 70% to 75% of the cesium exchanged on the film.

2.2 Batch Results

Batch testing was conducted to study cesium loading and regeneration of high surface area nickel foam electrodes. Cesium uptake was monitored with time and compared with the theoretical capacity based on integration of cyclic voltammograms in a sodium solution. Table 1 shows the results for cesium uptake by films initially in the reduced state $[\text{Na}_2\text{NiFe}^{\text{II}}(\text{CN})_6]$ from solutions initially containing 6 ppm and 8 ppm cesium. Cesium uptake was 70% to 80% complete after 1 h and reached equilibrium within 18 h. Under the conditions of the experiment, cesium loading reached 22% of the theoretical ion exchange capacity based on voltammetry. Similarly, experimental cesium capacities for nickel hexacyanoferrate powders are reported to be in the range of 23% to 46% of theoretical (Streat and Jacobi 1995).

Table 1. Actual and Theoretical Cesium Loading on 60 ppi Nickel Foam Electrodes. Theoretical Capacity Based on Integration of Cyclic Voltammograms in Sodium-Containing Solutions.

$[Cs]_0$	Time (h)	Actual Cs Loaded (moles/cm ²)	Theoretical Cs Loaded (moles/cm ²)	Actual/Theoretical (%)
6 ppm	1	5.6×10^{-9}	3.4×10^{-8}	16
	16	7.6×10^{-9}	3.4×10^{-8}	22
	24	7.1×10^{-9}	3.4×10^{-8}	21
8 ppm	1	5.7×10^{-9}	3.3×10^{-8}	17
	16	7.0×10^{-9}	3.3×10^{-8}	21
	24	7.2×10^{-9}	3.3×10^{-8}	22

Figure 8 shows cesium loading data for the 6 ppm and 8 ppm solutions with reduced films, as well as loading by an oxidized film and by an initially oxidized film with a cathodic (reducing) potential of 0.1 V (SCE) applied during uptake. The oxidized film $[NaNiFe^{III}(CN)_6]$ without applied potential loaded roughly half as much cesium as the reduced films. This is expected since the oxidized film contains half the number of exchangeable sodium atoms as the reduced film. However, application of 0.1 V (SCE) to an initially oxidized film results in loading to 90% of the level obtained for the reduced films within 1 h. Application of the potential accelerates cesium loading as the film is reduced (1 h data), but apparently does not affect the overall capacity of the film.

Batch tests were also conducted to determine the influence of sodium on cesium uptake. Figure 9 compares data for sodium-free cesium solutions with solutions containing Na/Cs molar ratios of 190 ($0.01 M Na^+$) and 17,000 ($1 M Na^+$). Sodium ion might slow the kinetics of cesium binding slightly since less was loaded after 1 h. However, after 24 h, very nearly the same loading was observed as when sodium was not present, with some depression by $1 M Na^+$ possibly indicated. The films on the high surface area electrodes appear to have the same high selectivity for cesium as films previously prepared on flat electrodes and the same as nickel hexacyanoferrate powders or packed beds.

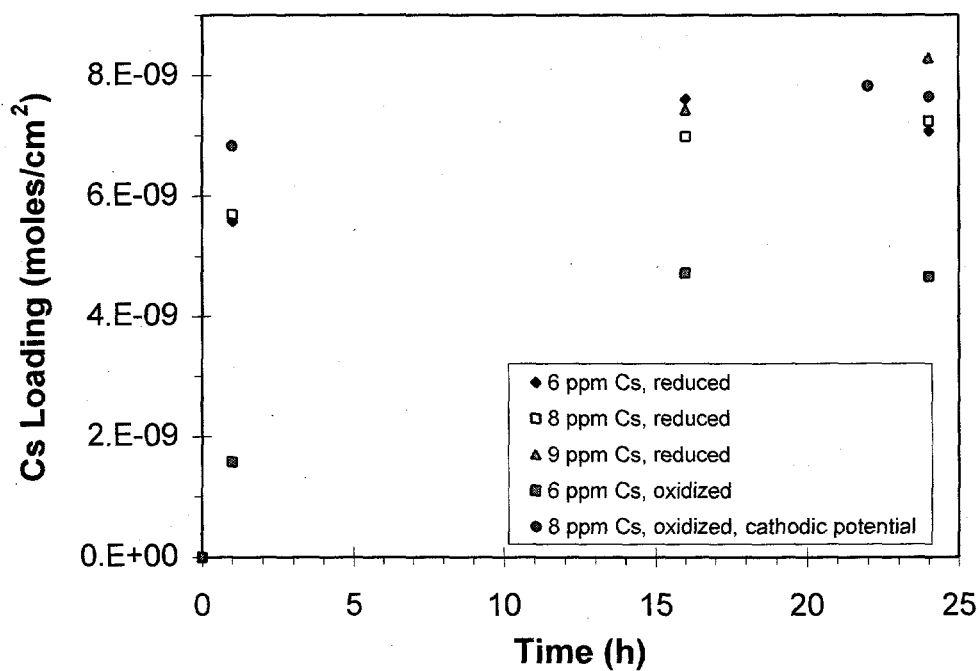


Figure 8. Effect of Applied Potential on Cesium Uptake in Batch Experiments

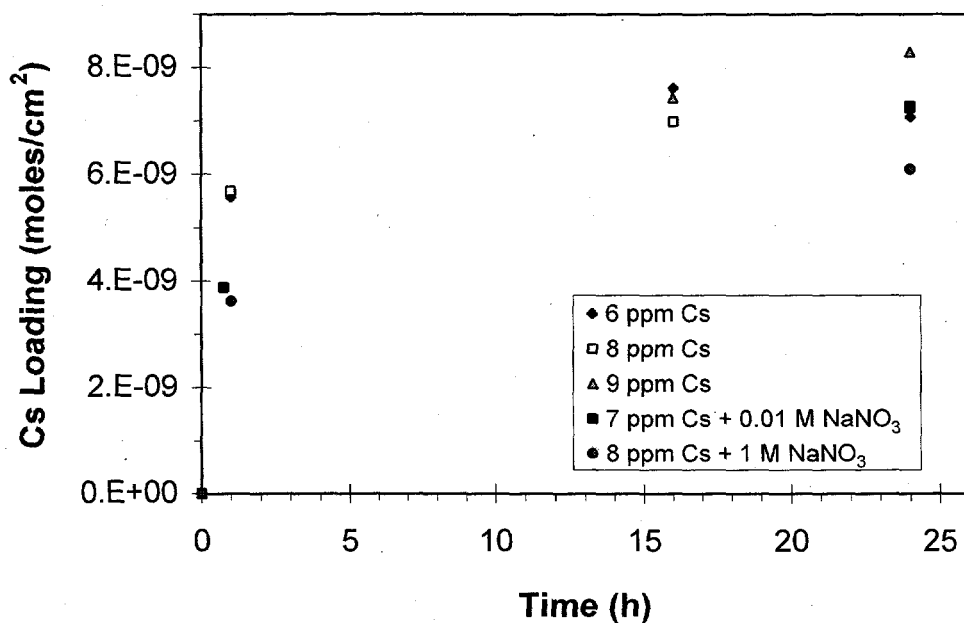


Figure 9. Effect of Sodium on Cesium Uptake in Batch Experiments

The effect of elution solution conductivity on unloading the films was investigated in batch tests. Conductive solutions appear to be best for unloading at an applied potential of 0.8 V (SCE), as shown in Figure 10. In an elution solution containing 1 M NaNO₃, the cesium in the film was fully unloaded after 10 min at this potential. However, films were only about 35% unloaded in 6 ppm cesium and about 25% unloaded in distilled water after 10 min. After 60 min in distilled water, films were 45% unloaded (not shown).

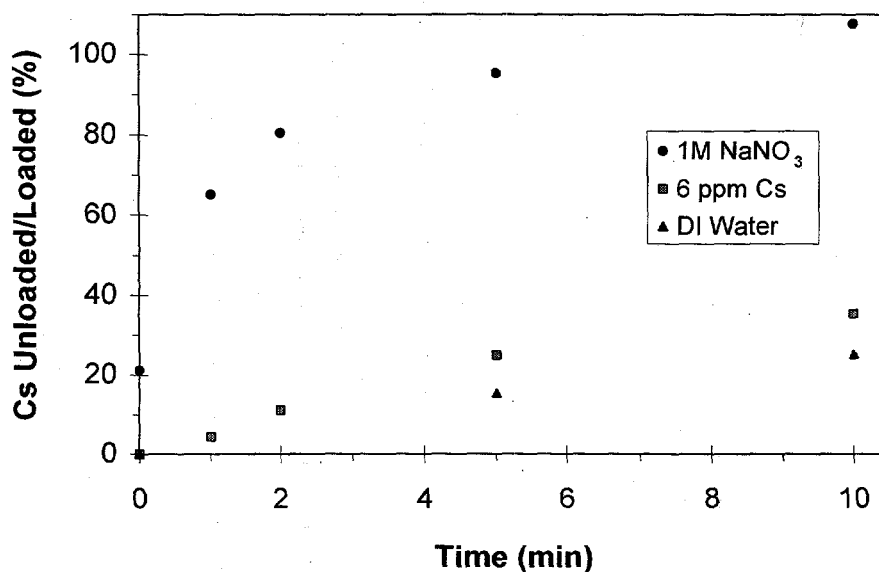


Figure 10. Effect of Elution Solution on Cesium Unloading in Batch Experiments (Applied Potential = 0.8 V)

2.3 Flow Cell Results

This section presents the results of studies to determine the performance of hexacyano-ferrate-modified nickel electrodes for the removal of cesium under flow conditions. Micro Flow cell tests (conducted by PNNL) of single and multiple stacked electrodes operated in flow-through mode are described here. An initial engineering evaluation is presented for an application at Hanford's KE Basin, based on the test results. Results of tests with an MP cell (conducted by The Electrosynthesis Co., Inc.) containing a single electrode operated in flow-by mode are also discussed in this section.

2.3.1 Micro Flow Cell Results Using a Single Electrode

Bench-scale flow experiments were conducted in which cesium uptake was measured as a function of flow rate and initial cesium concentration, [Cs]₀, for solutions passed through a 60 ppi nickel foam electrode upon which the electroactive film was deposited using the PNNL-2

method. Experiments reported here were conducted without applying a potential and in flow-through mode, in which solution was forced through the 2.8 cm x 2.1 cm face of the high surface area electrode, passing through the electrode thickness of 0.64 cm ("length/diameter," or l/d , = 0.3). Figure 11 shows breakthrough curves for a feed containing 0.2 ppm Cs as a function of flow rate. In nonradioactive testing, 0.2 ppm Cs was the lowest concentration that could be used due to cesium detection limits of approximately 0.02 ppm for atomic absorption analyses. At 13 BV/h, no breakthrough was observed until about 22 BV; 50% breakthrough occurred at 50 BV. Similar behavior was observed at slower flow rates, but breakthrough occurred immediately at the faster flow rates tested.

The breakthrough curves were well defined, even though the l/d was relatively low for the single electrode flow-through setup. The low l/d does not allow for fully developed flow, and some channeling and significant dispersion are expected.

Initial cesium concentration did not greatly affect breakthrough for $[Cs]_0$ of 0.12 and 0.18 ppm at a flow rate of 8 BV/h (Figure 12). Breakthrough occurred rapidly at a feed concentration of 0.38 ppm.

The flow studies show that films are stable up to the maximum flow rate tested of 113 BV/h. No significant decline in capacity or performance was observed throughout experimentation. Table 2 summarizes results of all Micro Flow cell testing, in the order experiments

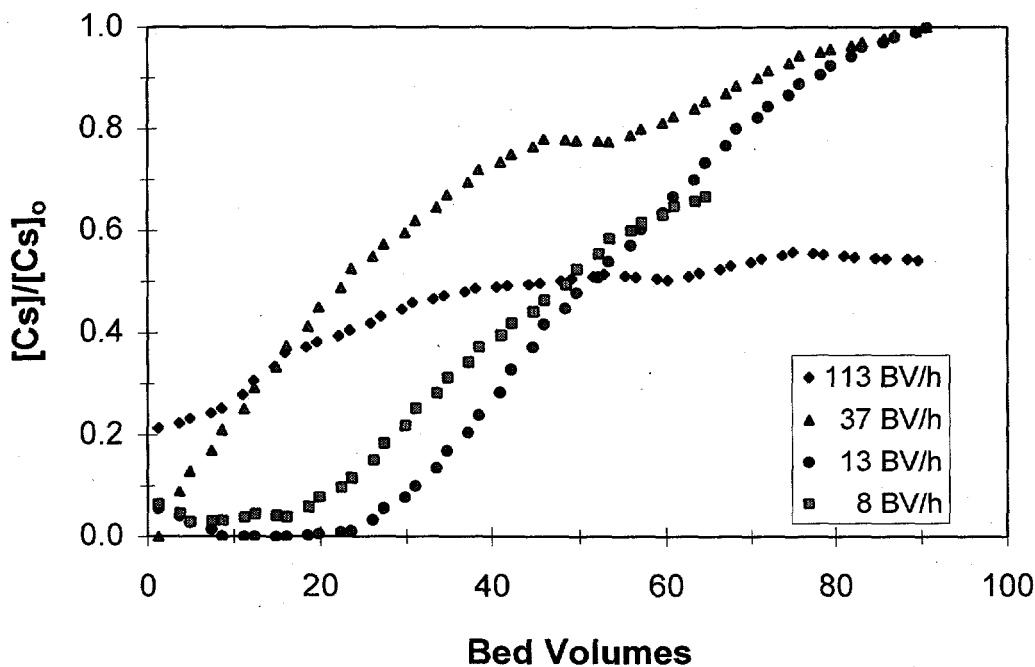


Figure 11. Effect of Flow Rate on Cesium Breakthrough in Flow-through Mode ($[Cs]_0 = 0.2$ ppm)

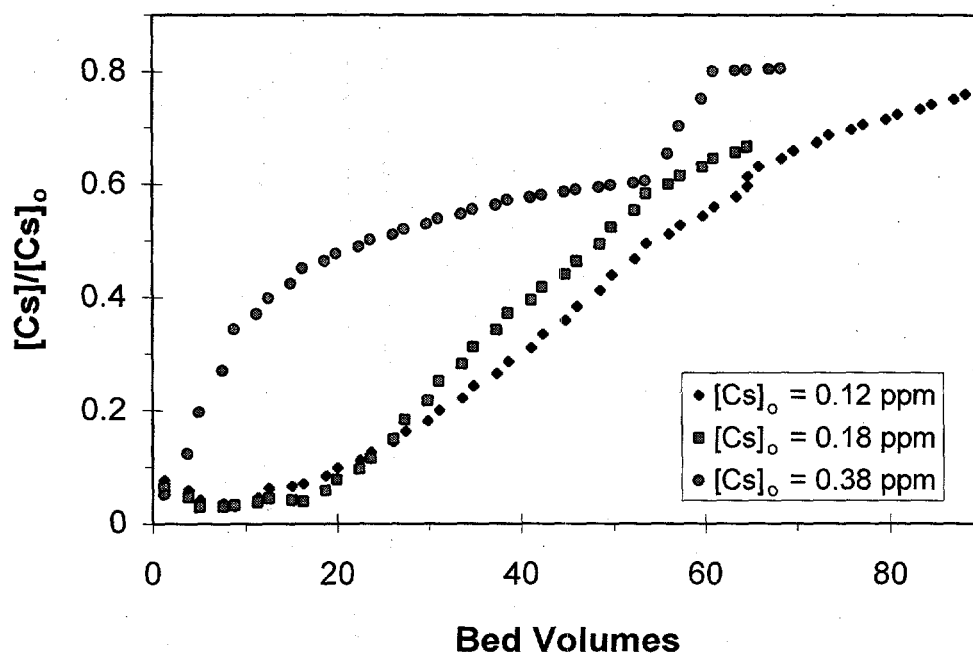


Figure 12. Effect of $[Cs]_0$ on Cesium Breakthrough in Flow-through Mode (Flow Rate = 8 BV/h)

Table 2. Summary of Results from Micro Flow Cell Tests

$[Cs]_0$	BV/h	Cs Loaded (moles/cm ²)	Cs Unloaded (moles/cm ²)	Theoretical [®] (moles/cm ²)	Loaded/Theoretical
0.18	112	1.6×10^{-9}	2.0×10^{-9}	1.8×10^{-8}	9 %
0.18	13	1.7×10^{-9}	2.6×10^{-9}	1.8×10^{-8}	9 %
0.20	37	1.1×10^{-9}	2.1×10^{-9}	1.7×10^{-8}	6 %
0.38	8	2.2×10^{-9}	2.2×10^{-9}	1.4×10^{-8}	16 %
0.17	8	1.4×10^{-9}	1.3×10^{-9}	1.4×10^{-8}	10 %
0.12	8	1.2×10^{-9}	1.2×10^{-9}	1.3×10^{-8}	9 %
[®] 0.20	13	1.9×10^{-9}	NA	2.2×10^{-8}	9 %

Electrode #1, in order of testing

② Na charge basis

③ Electrode #2

were conducted. While a slight drop is seen in the theoretical loading based on cyclic voltammetry in sodium solutions, the amount of cesium loaded remains about constant. The drop in theoretical loading results from the normal loss in capacity after the film has been subjected to the numerous redox cycles during the course of experimentation. Over the course of experimentation, the film maintained about a 10% efficiency in site utilization. This efficiency is about half that obtained in batch testing, which suggests that stacking the electrodes to give a longer bed depth may lead to improved performance and better utilization of film capacity. (Stacked electrode results are discussed in the following section.) Films were unloaded quantitatively, as indicated both by the amount of cesium unloaded compared with the amount loaded and by the consistency of the amount of cesium loaded from one run to the next.

Table 2 also shows that Electrode 2, a new electrode with a fresh film, performs the same as Electrode 1. The similarity in cesium breakthrough for these two electrodes is shown in Figure 13. These results are another indication of the consistency from one film deposition to the next.

2.3.2 Micro Flow Cell Results Using Stacked Electrodes

A stacked electrode configuration was used in the Micro Flow cell in order to increase the effective bed depth of the cell. Two sets of five 60 ppi electrodes, each electrode identical to that used in the single electrode tests, were coated with a hexacyanoferrate film (PNNL-2

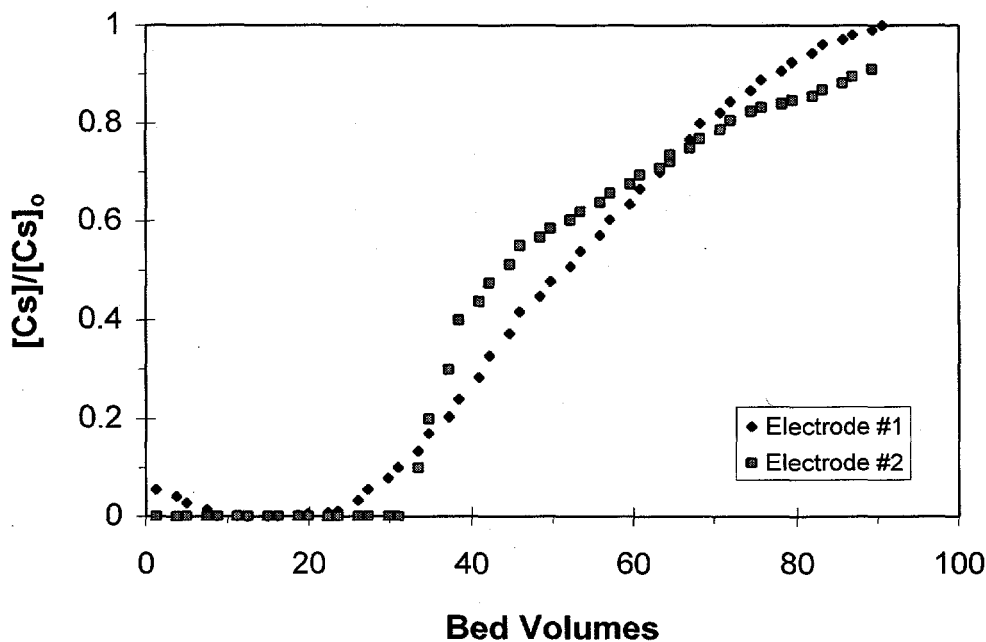


Figure 13. Consistency of Performance for Two Separate Electrodes in Flow-through Mode ($[Cs]_0 = 0.2$ ppm; Flow Rate = 13 BV/h)

method). One set of five electrodes was assembled in the cell such that solution flowed from the bottom of the cell up through the large face of each electrode in series (Figures 5 and 6). The bed depth, therefore, was five times that used in the single electrode experiments, or 3.18 cm (1.25 in), giving an l/d of about 1.5. As a result, the bed volume was also five times greater and the volumetric flow rates (mL/min) in the stacked cell were five times those used in the single electrode experiments at the same BV/h flow rates. Ion exchange experiments were conducted with regenerated films $[\text{Na}_2\text{NiFe}(\text{CN})_6]$ without application of a potential. The concentration of cesium in the feed, $[\text{Cs}]_0$, was 0.2 ppm in all tests.

The effect of flow rate on cell performance was determined. Figure 14 shows breakthrough as a function of flow rate. The results of two initial experiments at 13 BV/h and 37 BV/h are not shown because the experiments were only run for 100 BV and collected samples contained no detectable cesium; i.e., breakthrough was not observed. In subsequent experiments conducted for 200 BV, a flow rate dependence was observed that was similar to that obtained in single electrode experiments; higher flow rates gave faster breakthrough. At 113 BV/h (electrode Set 1), 37 BV/h (Set 2), and 13 BV/h (Set 2), onset of breakthrough occurred at about 60 BV, 90 BV, and 120 BV, respectively. Fifty percent breakthrough for 37 and 13 BV/h occurred at about 180 BV; for 113 BV/h, 50% breakthrough was at about 120 BV. This performance was much better than that seen for a single electrode at the same BV/h flow rates. For example, the best onset of breakthrough for a single electrode was 22 BV obtained at a flow rate of 13 BV/h; 50% breakthrough occurred at 50 BV under these conditions. The stacked cell

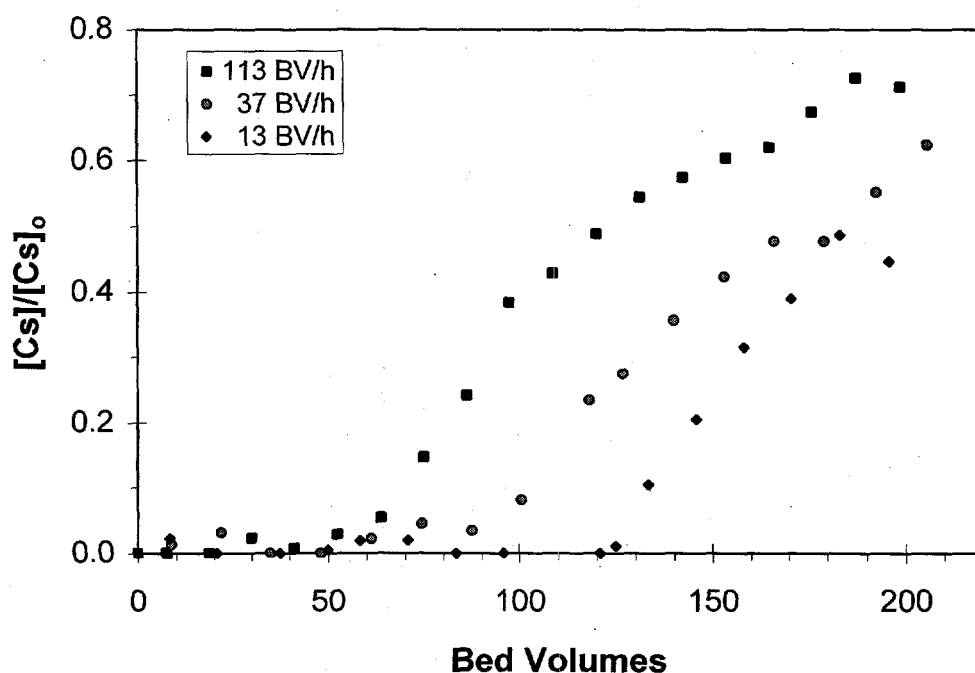


Figure 14. Effect of Flow Rate on Cesium Breakthrough in a Micro Flow Cell Containing Five Stacked Electrodes Operated in Flow-through Mode ($[\text{Cs}]_0 = 0.2$ ppm)

operated about five times more efficiently than the single electrode cell, presumably because the longer cell allows for more fully developed flow, minimizing channeling and dispersion. In addition, the first electrodes in the stack continued to absorb cesium throughout the experiment, reaching higher loading levels than were possible in the single electrode setup.

2.3.3 MP Results Using a Single Electrode

Experiments were conducted to investigate the performance of hexacyanoferrate-coated nickel foam electrodes in flow-by mode. The Electroynthesis Co., Inc., conducted these experiments in a commercial MP cell, using a 10 cm x 10 cm x 0.64 cm electrode, and investigated the effects of cesium concentration and flow rate on cesium uptake. In situ regeneration of the ESIX electrode was also studied. Their results are summarized here and reported in Appendix B.

Figure 15 shows plots of $[Cs]/[Cs]_0$ versus bed volumes of feed cesium solution for four cesium concentrations; Table 3 summarizes these data. All of these experiments were carried out using foams with similar loadings of $Na_2NiFe(CN)_6$ (equivalent to 10 to 15 mg cesium per electrode) as determined voltammetrically. In all cases, breakthrough occurred when approximately 10% of the cations in the film had been exchanged. The foam continued to exchange cesium after breakthrough, but the observed $[Cs]/[Cs]_0$ increased rapidly; typically the

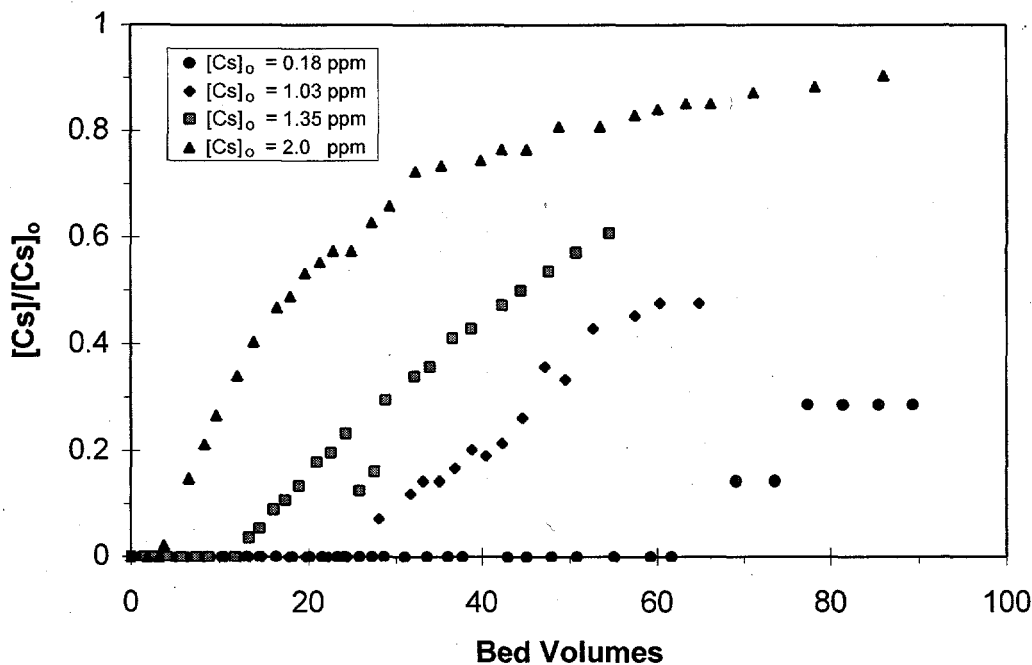


Figure 15. Effect of Feed Cesium Concentration on Cesium Breakthrough in an MP Cell Containing a Single Electrode Operated in Flow-by Mode

Table 3. Performance of 60 ppi Nickel Foam Electrodes in Flow-by Mode as a Function of Feed Cesium Concentration

<u>[Cs]₀</u> <u>(ppm)</u>	<u>Capacity</u> <u>(mg Cs)</u>	<u>Flow Rate</u> <u>(BV/h)</u>	<u>Bed volumes to</u> <u>[Cs]/[Cs]₀ = 0.1</u>	<u>Fractional loading</u> <u>at [Cs]/[Cs]₀ = 0.1</u>
2.0	10	11.3	6	0.08
1.35	14.4	8.6	17	0.10
1.03	15	8.2	27	0.12
0.18	13.8	8.5	65	0.06

Maximum film capacity based on voltammetry

exchange reached 20% to 30% before experiments were discontinued. It can be seen that, in this situation, the performance is very dependent on cesium concentration and the foam performance improves substantially as the concentration is decreased.

Several experiments were carried out with a cesium concentration of 0.2 ppm to study the effects of flow rate and film reproducibility. The results are summarized in Table 4. The effect of flow rate in the MP cell is not obvious from these experiments (60 ppi electrode). No clear trend relating flow rate and breakthrough was observed.

Generally, the experiments conducted with the 80 ppi electrode were carried out under similar conditions, and results show good reproducibility. It is clear, however, that a large change in film capacity does influence electrode performance. In the experiment with a thin film equivalent to only 4.4 mg of cesium, breakthrough occurred at a much lower solution volume compared with films of higher capacity (Table 4). Regardless of total capacity, breakthrough occurred at very similar values of fractional ion exchange.

The in situ elution of cesium from films on the nickel foam electrode by anodic oxidation was studied. The electrode reaction, shown in Eq. 1, will clearly lead to removal of a cation



from the film. Since the thermodynamics of binding of the cesium within the layer are more favorable than those for sodium, removal of the cesium by application of a potential step (as opposed to repeated potential cycling) is most likely to occur where, locally, within the layer, the fraction of cesium is high. As noted earlier, this will be the case close to the inlet to the foam and through the foam as more complete exchange is carried out during loading. During removal, some of the cesium could exchange back onto the film as the elution solution passes further down the foam towards the exit.

Table 4. Reproducibility and Flow Rate Dependence of Nickel Foam Electrodes in Flow-by Mode ($[Cs]_0 = 0.2$ ppm)

Porosity (ppi)	Capacity (mg Cs)	Flow Rate (BV/h)	Bed Volumes to $[Cs]/[Cs]_0 = 0.1$	Fractional Loading at $[Cs]/[Cs]_0 = 0.1$
60	13.8	8.5	65	0.06
	11.6	14.9	90	0.09
	13.8	18	110	0.10
	13.8	22.7	100	0.09
80	4.4	8.5	38	0.09
	16.7	8.2	100	0.07
	^② 16.7	8.7	80	0.07
	^② 16.7	8.7	120	0.10
	^② 16.7	22.6	80	0.06
	^② 16.7	8.8	80	0.06

Maximum film capacity based on voltammetry

^② Capacity of original film; capacity not measured after in situ regeneration

Four experiments were carried out where an 80 ppi nickel foam ESIX electrode (initial cesium capacity equivalent to 16.7 mg) was loaded to an extent of 15% to 20% with cesium, using a solution containing 0.2 ppm cesium. These experiments correspond to the last four shown in Table 4. The cesium-loaded foam was then oxidized using a constant current of 5 mA while passing a solution of 0.1 M NaNO₃ (300 mL) through the foam at a flow rate of 1 mL/s. The eluant was about 3 ppm in cesium, and the total recoveries of cesium were between 60% and 80%. The bed performance for cesium uptake was not greatly altered after each regeneration cycle, as indicated by the consistent breakthrough and fractional loading data in Table 4.

These experiments were all conducted with a current of 5 mA, a very low current density. The low current was employed in these preliminary experiments to avoid possible competing electrode reactions such as oxygen evolution. However, the voltammetric response suggests it would be possible to discharge most of the cesium at a much higher rate, speeding regeneration, giving a higher cesium concentration in the eluant, and affording a higher concentration factor.

2.4 Modeling of Micro Flow Cell and MP Cell Data

With the Micro Flow cell and MP cell data presented above as a basis, the expected performance of ESIX to treat wastes can be estimated using the following expression developed for conventional ion exchange (Hiester and Vermeulen 1952; Thomas 1944).

$$\frac{c}{c_0} = \frac{J(RS, T)}{J(RS, T) + e^{(R-1)(T-S)} [1 - J(S, RT)]} \quad (2)$$

where $S = \frac{\kappa a V \varepsilon}{Q}$ is the column capacity parameter, $T = \frac{\kappa a (Q t - V \varepsilon)}{D_G Q}$ is the solution capacity parameter, $D_G = \frac{q_M}{c_0 \varepsilon}$ is the column distribution ratio, $R = \frac{1}{K}$ and $K = \frac{(c_0 - c)q}{c(q_M - q)}$ is the

equilibrium constant, c_0 is the Cs concentration at the inlet, q_M is the maximum concentration of exchangeable ions in the solid matrix, c is the Cs concentration in solution, q is the concentration of Cs in the solid matrix, ε is the porosity of the solid matrix, κa is the overall mass transfer coefficient, V is the reactor volume, t is time, and Q is the solution flow rate. The function J is the zeroth order Bessel function for a purely imaginary argument,

$$J(x, y) = 1 - \int_0^x e^{-y-\xi} I_0(2\sqrt{y\xi}) d\xi \quad (3)$$

For the limiting condition where the film is very selective for Cs (or equivalently, $K \rightarrow \infty$), which is the case here as shown earlier with the batch results, the expression above simplifies to Eq. 4:

$$\frac{c}{c_0} = \frac{1}{1 + e^{S-T} (1 - e^{-S})} \quad (4)$$

From the definitions of S and T above, the only free parameters are κa and q_M . V , ε , Q , and c_0 are all fixed at the outset. To verify the applicability of the expression above in describing the ESIX system, two sets of comparisons were carried out: 1) verify that velocity scales appropriately and 2) verify that concentration scales correctly.

To verify the velocity scaling, experimental data for the three flow rates collected using the 5-stack configuration were used. The results from the 5-stack configuration are preferred over the results obtained using the 1-stack configuration since the 5-stack configuration resembles conventional ion exchange systems more closely and entrance effects and dispersion are less pronounced for the longer bed depth.

The two free parameters, κa and q_M , were determined by fitting Eq. 4 to one experimental set. Once these parameters were determined, Eq. 4 was used to predict the breakthrough curves for conditions used in the other experimental sets. The results are shown in Figure 16, where the data obtained at 13 BV/h were used to determine the parameters. The results clearly show that the model does not describe the experimental data very well; specifically, the model predicts immediate breakthrough for both 37 and 113 BV/h flow rates. It should be noted, however, that in using the parameters obtained from fitting the data at 13 BV/h to estimate the breakthrough curves for flow rates of 37 BV/h and 113 BV/h, both κa and q_M were assumed to be independent of the flow rate. While q_M is not expected to depend on the flow rate, κa contains the mass transfer coefficient of the liquid side, which depends on the flow rate. In particular, the mass transfer coefficient in the liquid side has been reported to scale with the superficial velocity (v) raised to the power of 0.39 (Montillet et al. 1994), 0.61 (Montillet et al. 1994), and 0.7 (Brown et al. 1994).

Scaling the mass transfer coefficient with the superficial velocity yielded better agreement between the model and the experimental results, as shown in Figures 17 ($\kappa a \propto v^{0.39}$), 18 ($\kappa a \propto v^{0.61}$), and 19 ($\kappa a \propto v^{0.70}$). The agreement, while still not completely accurate for all flow rates, seems to be best when the superficial velocity is raised to the 0.39 power. The two main conclusions are 1) a conventional ion exchange model describes the process reasonably well, and 2) mass transfer resistance in the liquid side cannot be dismissed *a priori*. We believe that the discrepancies seen between the model and the experimental results are due at least in part to using a second set of electrodes at the fastest flow rate, as well as dispersion and channeling effects. While channeling and dispersion effects seem to play a role in the 5-electrode stack, the effects were apparently larger in the single electrode stack since modeling results could not be extrapolated as accurately to other flow rates. We are currently studying these effects further. (It should be noted that the choice of which data set is used to determine the parameters is arbitrary, and if another data set is chosen, the results are qualitatively similar to those shown in Figures 16 through 19.)

To verify the scaling of inlet concentration, three sets of concentration dependence data from MP cell testing were used (Table 3, $[Cs]_0 = 0.18, 1.03, \text{ and } 1.35 \text{ ppm}$). These sets were chosen simply because they had similar experimental conditions with the exception of the inlet concentration. The 1.03 ppm data were used to determine the parameters as before, and they were in turn used to calculate the expected breakthrough curves for the other two data sets. The results are shown in Figure 20. It can be seen that the model predicts the inlet concentration effects qualitatively.

These initial modeling efforts provide a good basis for system scale-up and extrapolation of ESIX performance in treating wastes, including KE Basin water, which is discussed in Section 2.5. Additional model development and experimental testing to eliminate dispersion and channeling effects are planned and are necessary to more fully understand the ESIX system.

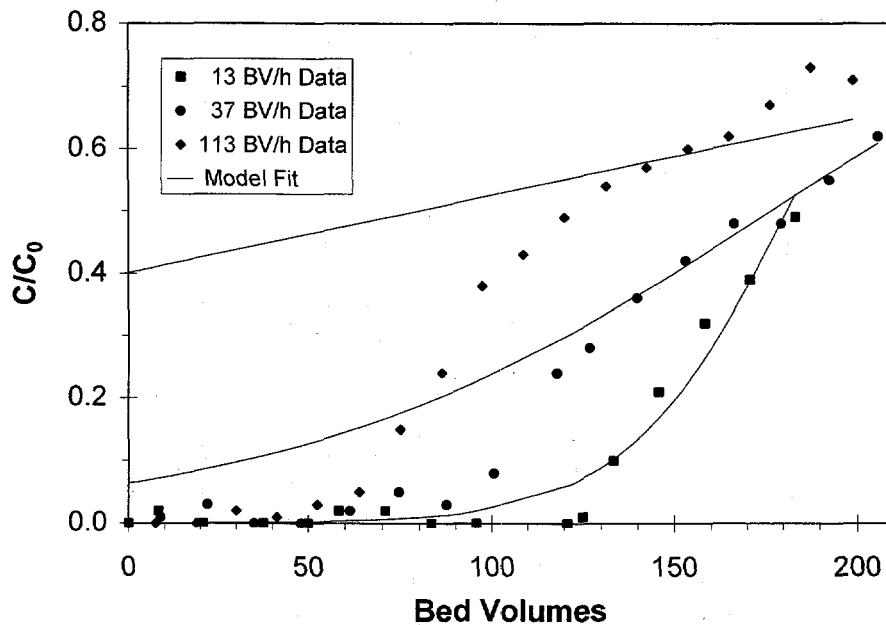


Figure 16. Model Fit to Breakthrough Data for $[Cs]_0 = 0.2$ ppm and Flow Rate = 13, 37, and 113 BV/h in Flow-through Mode for Five Stacked Electrodes

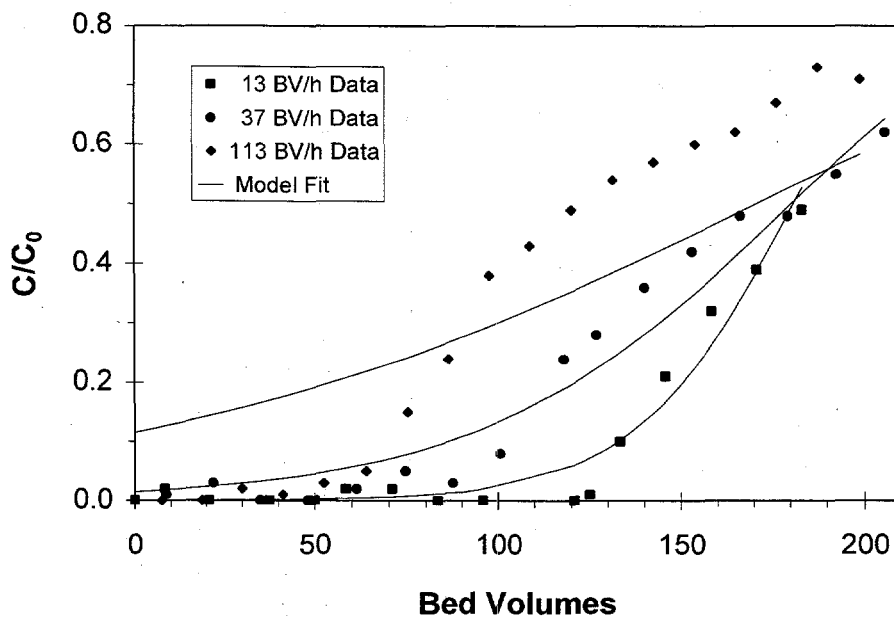


Figure 17. Model Fit to Breakthrough Data for $[Cs]_0 = 0.2$ ppm and Flow Rate = 13, 37, and 113 BV/h in Flow-through Mode for Five Stacked Electrodes. Model Calculated for $\kappa a \propto v^{0.39}$

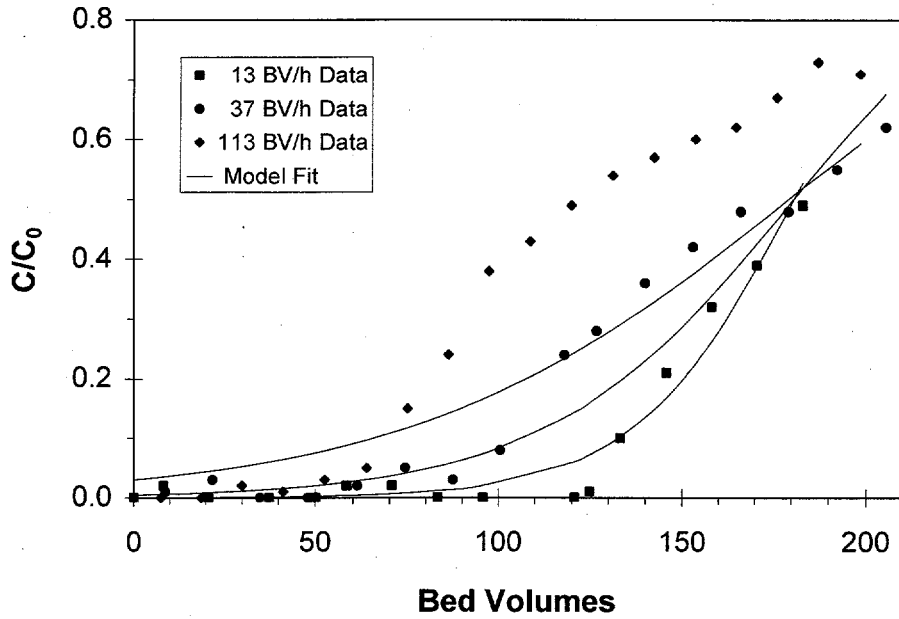


Figure 18. Model Fit to Breakthrough Data for $[Cs]_0 = 0.2$ ppm and Flow Rate = 13, 37, and 113 BV/h in Flow-through Mode for Five Stacked Electrodes. Model Calculated for $\kappa a \propto v^{0.61}$

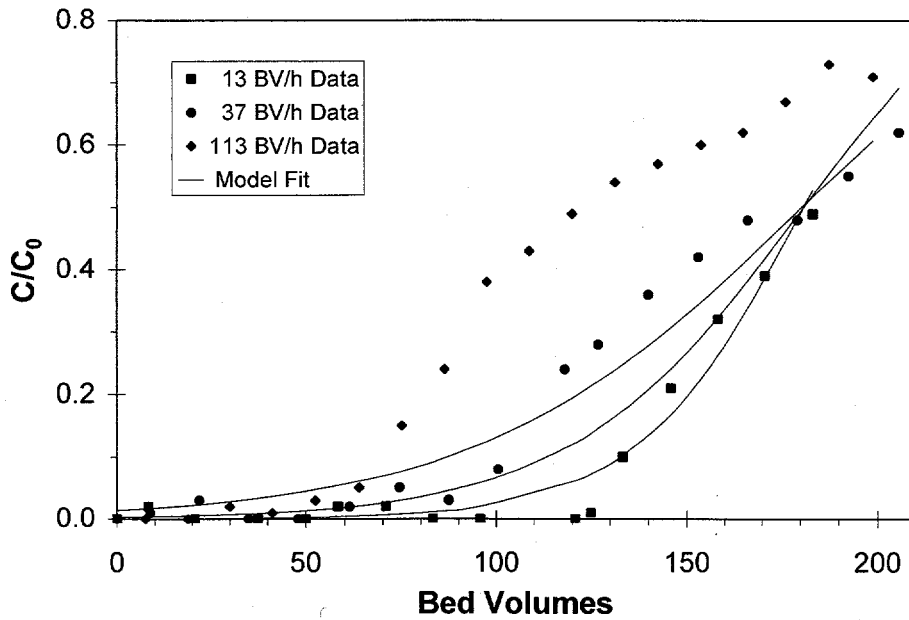


Figure 19. Model Fit to Breakthrough Data for $[Cs]_0 = 0.2$ ppm and Flow Rate = 13, 37, and 113 BV/h in Flow-through Mode for Five Stacked Electrodes. Model Calculated for $\kappa a \propto v^{0.7}$

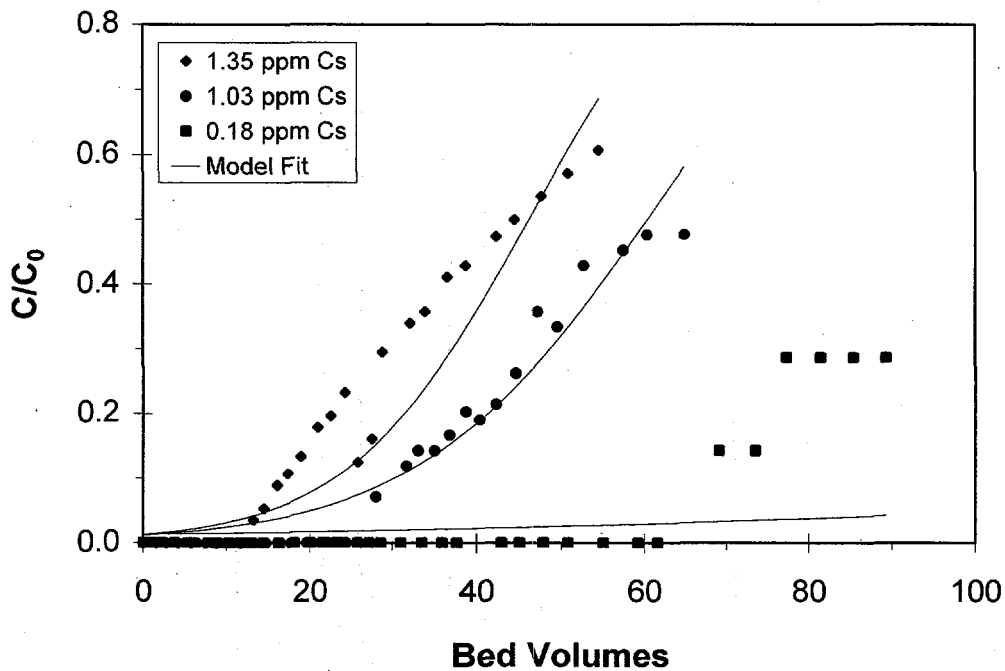


Figure 20. Model Fit to Breakthrough Data for Flow Rate = 8.5 BV/h and $[Cs]_0 = 0.18, 1.03, 1.35$ ppm and in Flow-by Mode for a Single Electrode

2.5 ESIX Case Study for KE Basin Application

Results are presented here for a case study for cesium removal from KE Basin. The case study shows considerable savings in capital expenditures, as well as decreased costs for secondary waste disposal. While estimates are based on KE Basin, results are expected to also be comparable to the cost savings and reduced secondary waste volumes attainable for the other waste feeds listed in Section 1.3 (Target Applications), where conventional ion exchange is used to remove the cesium.

2.5.1 Bases and Assumptions

Experimental data from the Micro Flow cell tests, conducted by PNNL, were used to predict the breakthrough characteristics for KE Basin feeds. A model was used to fit breakthrough data obtained during the Micro Flow cell testing in both the single and stacked electrode configurations. The results are plotted in Figure 21. Model parameters were then applied to the range of concentrations of cesium encountered in KE Basin (10^{-7} M near the bottom, and 10^{-10} M near the top), assuming the same flow rate (BV/h) would be used in the scaled-up system. Figure 22 shows the predicted column performance using both the single and stacked electrode data as a basis. For the 5-electrode stacked configuration, 50% breakthrough is

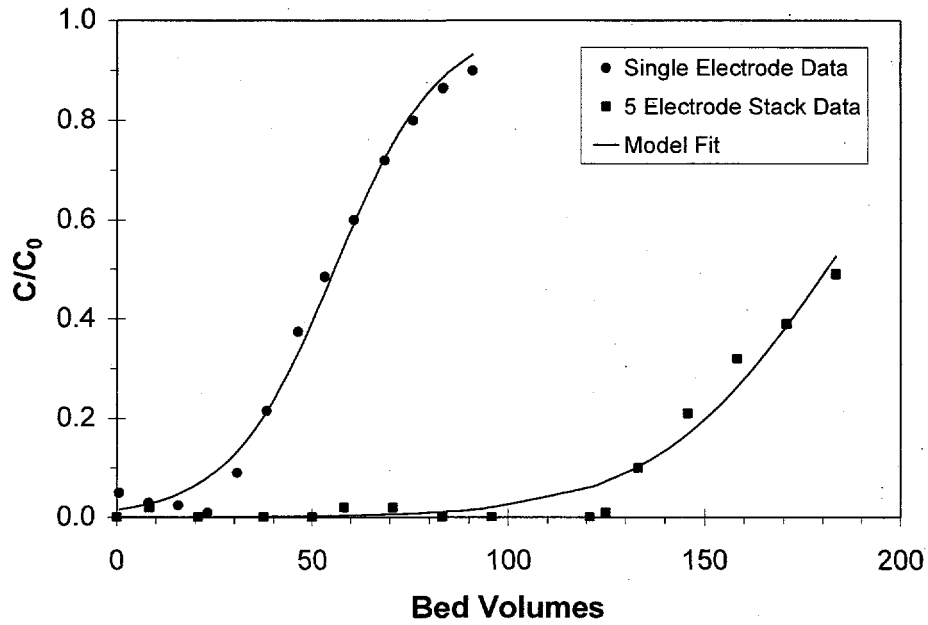


Figure 21. Model Fit to Breakthrough Data for $[Cs]_0 = 0.2$ ppm and Flow Rate = 13 BV/h in Flow-through Mode for Single and Stacked Electrodes

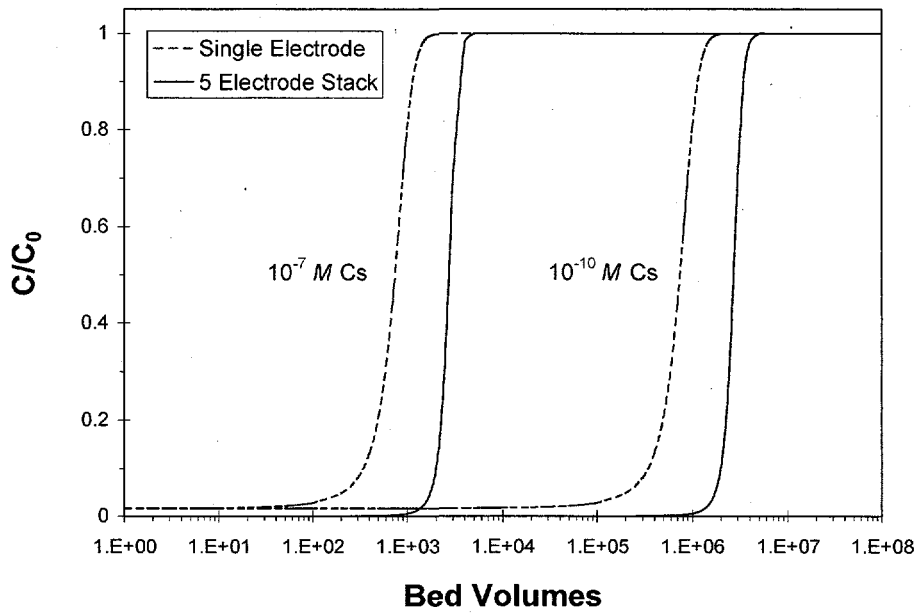


Figure 22. Predicted Breakthrough for ESIX Treatment of KE Basin Water at 13 BV/h for Feeds of 10^{-7} and 10^{-10} M Cs

expected to occur after 3×10^3 to 3×10^6 BV for the highest and lowest concentrations, respectively. Since the 5-electrode stacked testing showed marked improvement over the single electrode testing, and since the stacked electrode configuration is more representative of the configuration of a scaled-up system, the modeling results obtained from the 5-electrode stacked testing were used to predict the performance of a scaled-up system.

The modeling results obtained from the Micro Flow stacked cell tests were combined with conservative (worst-case) design baseline parameters for film deposition, film regeneration, cesium loading, and cesium elution, most of which were based on experimental results. The engineering bases were that the electroactive film would be deposited after every 1500 load/unload cycles; film regeneration would take 10 min (or less) with an applied potential of 0.1 V (SCE); the nominal film capacity is 1.7×10^{-9} moles Cs/cm² electrode surface area; loading would be carried out by ion exchange without application of a potential; elution would take 10 min at an applied potential of 0.8 V; the average concentration of the waste stream is 1×10^{-9} M Cs (slightly higher than the cesium concentration currently being processed); a flow rate of 400 L/min is required; cesium would be eluted just before the predicted onset of breakthrough rather than 50% breakthrough, and, 2 BV of rinse solution would be required after each elution.

For the KE Basin processing, the ESIX system would be used in semi-continuous batch recycle mode, as shown in Figure 23. This same mode of operation is currently conducted via conventional ion exchange to minimize worker exposure to cesium by maintaining a low "steady

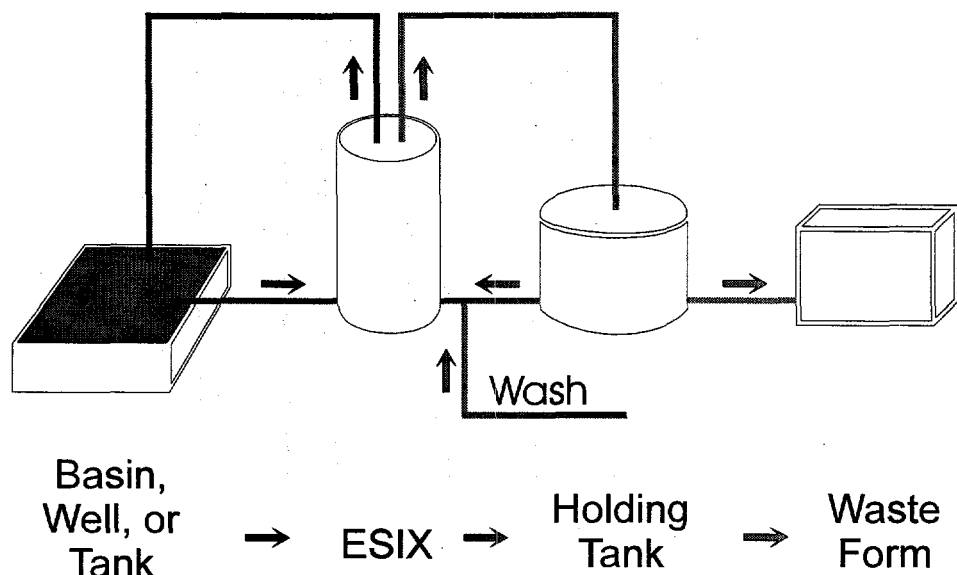


Figure 23. Flow Diagram for Waste Decontamination with ESIX

state" cesium concentration in the basin. Basin water (or other feed) would be passed through the ESIX column until the onset of breakthrough. The system could also be used in single-pass operation for final water decontamination or in applications in which batch recycle is not desired or feasible. When the column reaches capacity, the feed to the system is stopped. Cesium is then eluted into an elution solution, which is pumped through the system from a holding tank. The elution solution can be reused several times until a limiting (i.e., heat load, radiation constraints, etc.) final cesium concentration is reached.

For this analysis, it was assumed that the elution solution would be disposed of after 10 elution cycles; however, more could possibly be accommodated, depending on the desired composition of the final waste cesium product. A wash solution, needed to remove residual cesium for improved process efficiency, could be added to the holding tank after each wash. Alternately, the wash solution could be kept separate, reused until a threshold concentration is reached, and used later as the next elution solution. The elution solution is periodically transferred from the holding tank to the final waste form.

2.5.2 Process Concept and Estimated Costs

The ESIX system would consist of 40 production modules. Each production module would contain 20 ESIX electrodes (60 ppi nickel foam) with an associated mesh counter electrode. Production modules could be arranged in two parallel series of 20 each as shown in Figure 24. The electrode volume in each production module would be approximately 0.05 m^3 , and the surface area would be 200 m^2 . The total ESIX system working electrode volume would be approximately 2 m^3 .

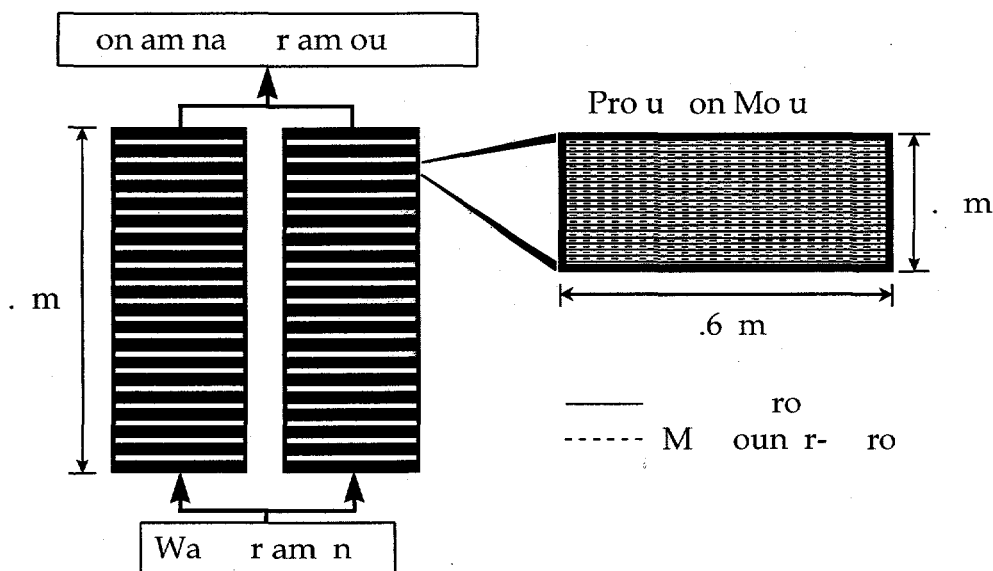


Figure 24. Conceptual Schematic Electrode Arrangement for KE Basin Decontamination

Given the above bases and flow diagram, 96,000 BV of waste would be processed before elution of the ESIX system is required. This corresponds to approximately 2×10^8 liters of waste processed and 330 days processing time for each load cycle. Over 7 years of continuous operation (assumed KE Basin baseline), approximately eight load/elution cycles would be required; thus, film redeposition would not be required.

An "order of magnitude" capital cost of \$2 M is estimated for the 40 production modules. Each production module (containing the 20 ESIX electrodes and mesh counter electrodes) would cost on the order of \$50,000 each. This estimate only includes the production modules and electrodes, which are anticipated to be the major equipment costs associated with the system. Costs associated with radiological applications are not included in this estimate.

2.5.3 Potential Advantages of ESIX for KE Basin Application

The ESIX system could have several significant advantages over current operations. Secondary waste would be reduced at least by a factor of 17. Current processing requires disposal of ion exchangers every month. Waste from this source totals approximately 80 m^3 with a disposal cost of \$150 K to \$300 K/year (assuming disposal costs of \$1800 to \$3600/ m^3 for LLW). Reusing the elution solution 10 times and assuming a 2 BV rinse volume, the ESIX system is estimated to generate 4.6 m^3 of secondary waste, costing just \$8 K to \$16 K/year for the same LLW disposal. Costs for ESIX could be even lower if the elution solution is used more than 10 times and if the rinse solution is reused as the next elution solution. Replacement costs of exchangers in the current system are estimated to be \$1.2 M/year. The ESIX system requires a one-time capital outlay of on the order of \$2 M, having a payback period of approximately 1-2 years. Labor costs and worker exposure might also be less since the current monthly column changeout is not needed for the ESIX system. Worker exposure could also be lower with ESIX because automated or remote operations may be possible.

Another potential advantage of ESIX is that loading with TRU is not expected to be a problem. Unlike the deep-bed filtration of colloidal TRU, which plagues standard ion exchange columns, TRU is less likely to accumulate on the open pore structure of the ESIX electrodes. If a small amount of TRU hangs up on the ESIX column during loading, it still may not contaminate the cesium product during elution. Elimination of TRU in the final waste allows higher cesium loading and less waste volume.

3.0 Conclusions

Experimental results support the viability of once-through or batch recycle waste processing with ESIX for cesium removal. Electroactive films on high surface area electrodes are stable to solution flow; have high selectivity for cesium in the presence of at least 2×10^4 molar excess of sodium ion; can be cycled through load/unload cycles up to 1500 times; can be efficiently eluted in-line; and have sufficient capacity to support a cesium separation process. Results from bench-scale experiments for single electrodes ($l/d = 0.3$) and 5-electrode stack in the flow-through configuration ($l/d = 1.5$) show that the stacked configuration has significantly improved breakthrough characteristics. In addition, single electrodes in the flow-by configuration show better performance than a single electrode in the flow-through configuration. This is presumably because the larger l/d values allow for more fully developed flow, minimizing channeling and dispersion.

From the design baseline parameters derived from current processing knowledge and experimental results, a concept for an economical remediation system has been devised and presented. A case study for continuous processing of KE Basin wastewater shows the potential for significant reduction of secondary wastes and associated disposal costs, and decreased capital and labor expenditures. Other processing improvements with ESIX include less likelihood of TRU contamination; decreased worker exposure because of less contact with exchangers and process hardware; and production of a cesium product containing a minimal amount of sodium, which would be compatible with a wider variety of final waste forms.

4.0 References

- Bocarsly, A. B., and S. Sinha. 1982. "Chemically Derivatized Nickel Surfaces: Synthesis of a New Class of Stable Electrode Interfaces." *Journal of the Electroanalytical Chemistry and Interfacial Electrochemistry* 137:157.
- Hiester, N. K., and T. Vermeulen. 1952. "Saturation Performance of Ion-Exchange and Adsorption Columns." *Chemical Engineering Progress* 48:505.
- Kurath, D. E., L. A. Bray, K. P. Brooks, G. N. Brown, S. A. Bryan, C. D. Carlson, K. J. Carson, J. R. DesChane, R. J. Elovich, and A. Y. Kim. 1994. *Experimental Data and Analysis to Support the Design of an Ion-Exchange Process for the Treatment of Hanford Tank Waste Supernatant Liquids*. PNNL-10187, Pacific Northwest National Laboratory, Richland, Washington.
- Lehto, J., and R. Harjula. 1987. "Separation of Cesium from Nuclear Waste Solutions with Hexacyanoferrate(II)s and Ammonium Phosphomolybdate." *Solvent Extraction and Ion Exchange* 5:343.
- Lilga, M. A., R. J. Orth, J. P. -H. Sukamto, D. T. Schwartz, S. M. Haight, and D. Genders. 1996. *Electrically Switched Cesium Ion Exchange. FY 1996 Annual Report*. PNNL-11441, Pacific Northwest National Laboratory, Richland, Washington.
- Montillet, A., J. Legrand, J. Comiti, M. M. Letord, and J. M. Jud. 1994. "Using of Metallic Foams in Electrochemical Reactors of Filter-Press Type: Mass Transfer and Flow Visualisation." in *Electrochemical Engineering and Energy*, F. Lapique, A. Storck, and A. A. Wragg, Eds. Plenum Press, New York.
- Brown, C. J., D. Pletcher, F. C. Walsh, J. K. Hammond, D. Robinson. 1994. "Studies of Three-dimensional Electrodes in the FM01-LC Laboratory Electrolyzer." *J. Applied Electrochem.* 24:95.
- Streat, M., and D. L. Jacobi. 1995. "Complex Hexacyanoferrates for the Removal of Cesium from Solution." In *Ion Exchange Technology*, A. K. Sengupta, Ed. Technomic, Lancaster, Pennsylvania, p. 193.
- Thomas, H. C. 1944. "Heterogeneous Ion Exchange in a Flowing System." *Journal of the American Chemical Society* 66:1664.

Appendix A

Development of ESIX Films Selective for Pertechnetate

Appendix A

Development of ESIX Films Selective for Pertechnetate

This work supported by Laboratory Directed Research and Development (LDRD) funding under the Pacific Northwest National Laboratory Science Technology for Environmental Processing (STEP) initiative.

The use of an electroactive material to selectively extract perrhenate ion (ReO_4^-) (surrogate for pertechnetate [TcO_4^-]) in the presence of high nitrate ion (NO_3^-) concentration has been investigated¹. As with the cesium separation process under development, a number of issues need to be resolved to determine the economic feasibility of the electrically switched anion exchange concept: 1) selectivity, 2) stability, and 3) capacity. Recent studies have addressed these issues in part, with a primary emphasis on selectivity. Selectivity of the electroactive material for ReO_4^- was established by examining the cyclic voltammograms and the associated mass loading of the material in solutions containing only NO_3^- , only ReO_4^- , and mixtures of the ions. The electroactive material was deposited as a film on a conducting substrate for these studies.

Typical results of cyclic voltammetry experiments are shown in Figures A1 and A2. The voltammograms show that both the anodic and cathodic peaks shift towards more negative potentials with higher concentrations of ReO_4^- . In Figure A1, selectivity for ReO_4^- is clearly seen by comparing the voltammograms obtained in the mixture and pure ReO_4^- . These two voltammograms essentially overlap, indicating almost complete selectivity for perrhenate over nitrate in the equimolar solution. The series of voltammograms shown in Figure A2 provide additional evidence. Initially, the film was cycled in pure nitrate and then the solution was

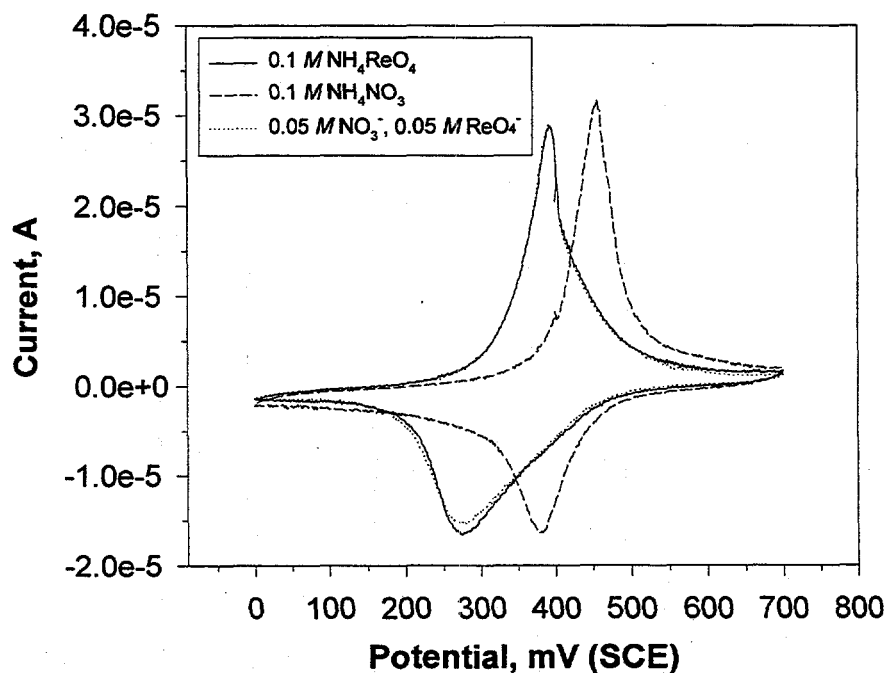


Figure A1. Cyclic Voltammograms of a ReO_4^- Selective Material in Various Solutions

¹ This work was funded at the Pacific Northwest National Laboratory through the Science and Technology for Environmental Processing (STEP) initiative.

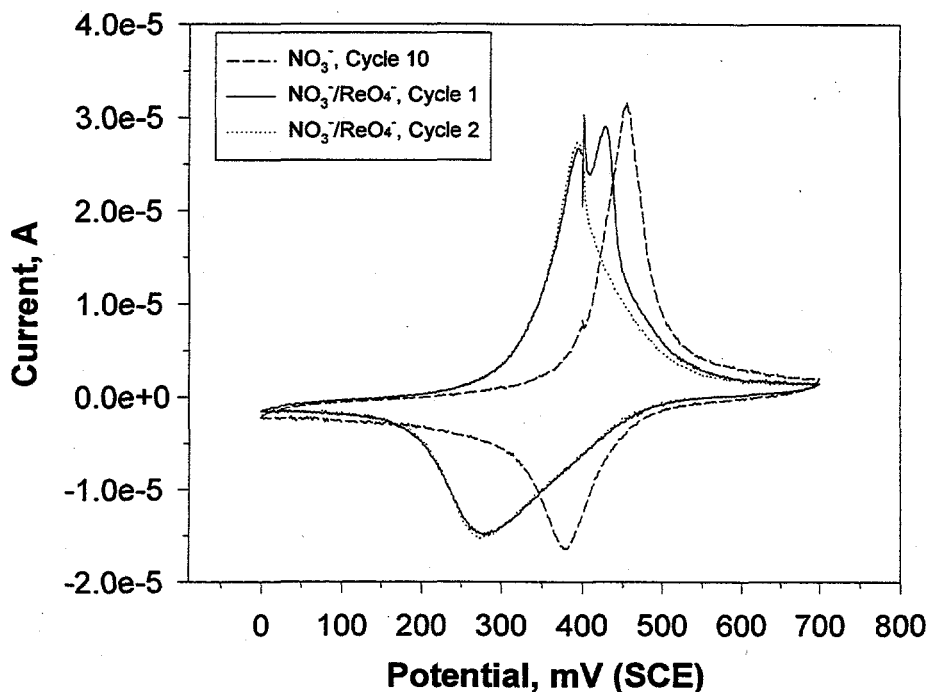


Figure A2. Cyclic Voltammograms Show Displacement of NO_3^- by ReO_4^-

changed to the equimolar mixture. During the first cycle in the mixture, peaks for both NO_3^- and ReO_4^- are observed in the voltammogram. During the second cycle in the mixture, only peaks associated with perrhenate are detected. In order to confirm and attempt to quantify the selectivity, the cyclic voltammograms were examined in conjunction with mass loading data.

Typical mass loading or Quartz Crystal Microbalance (QCM) results are shown in Figure A3. In the QCM technique a quartz crystal electrode is loaded with film, and the frequency at which the electrode oscillates is indicative of the mass loading. An increase of frequency is indicative of mass loss, and a decrease of frequency is associated with a mass increase. The data in Figure A3 are plotted as mass loading (arbitrary scale) as a function of the applied potential for three solutions, and these data correspond to the cyclic voltammograms shown in Figure A1. The QCM data show that in all three solutions (pure NO_3^- , pure ReO_4^- , and an equimolar mix) oxidation of the electroactive material, which corresponds to intercalation of anions, results in a mass increase in the film. The magnitude of the mass change during a cycle in pure nitrate solution is roughly one-fourth the observed mass change per cycle in the pure and mixed ReO_4^- solutions. This mass loading ratio is in good agreement with the ratio of nitrate to perrhenate molecular weights (62.0 g/mole:250.2 g/mole). This again suggests that perrhenate is selectively loaded by the material from a solution mixture.

Additional experiments are needed to quantify the degree of selectivity of the material for ReO_4^- over NO_3^- and to address the issues of film stability and capacity.

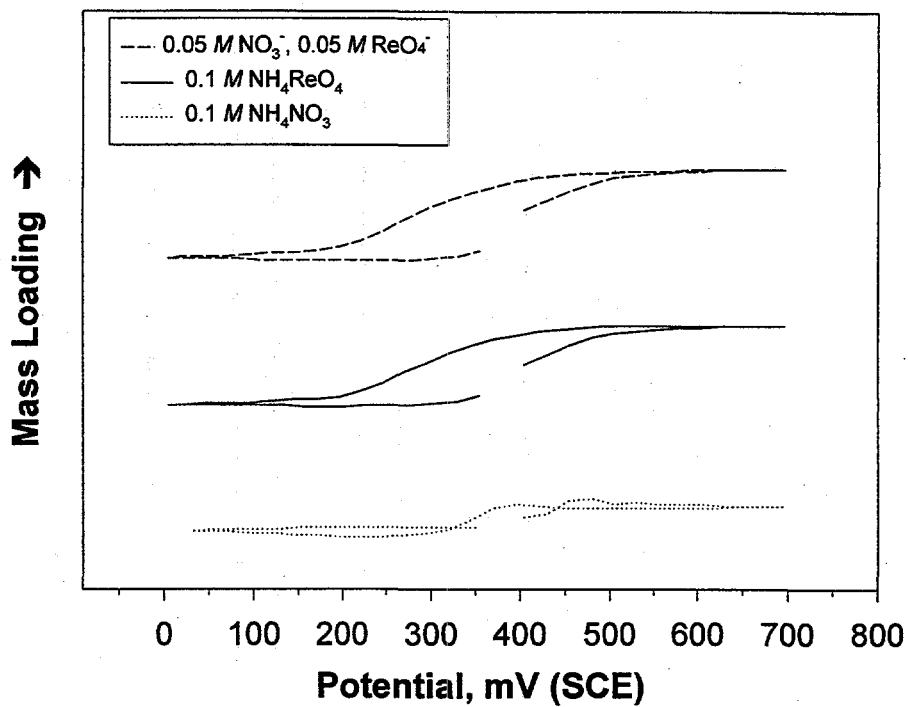


Figure A3. QCM Data Indicate Greater Mass Loading in the Presence of ReO_4^- (Note: the curves for mixed and pure ReO_4^- have been arbitrarily separated vertically for clarity.)

Appendix B

Contractor Report

Electrochemically Switched Ion Exchange

Appendix B

Contractor Report

Electrochemically Switched Ion Exchange

Dr. David Genders
Dr. Ram Gopal
The Electrosynthesis Company, Inc.
72 Ward Road
Lancaster, NY 14086-9779

Executive Summary

Previous work at Pacific Northwest National Laboratory on Electrically Switched Ion Exchange (ESIX) has been extended by studying the scale up of the process to a small commercial reactor, the MP cell from ElectroCell AB. The cell has been modified to include a Ni foam (dimensions 100 mm x 100 mm x 6.3 mm, volume 63 cm³) and good quality Na₂NiFe(CN)₆ films have been uniformly deposited. The resulting reactor has been tested using streams with various concentrations of Cs⁺ and using once-through flow. Its initial performance is good but this then decays. In order to understand the reasons, the reactor has been modelled and the model has been shown to fit the experimental data well.

The behavior of the reactor can be understood in terms of a model which includes the role of mass transfer and the deactivation of the Na₂NiFe(CN)₆ film as the Na⁺ cations within the layer are replaced by Cs⁺. The model stresses the role of mass transport in determining the minimum path length, L_{crit}, of the solution through the foam necessary to make possible the desired extent of removal of Cs⁺ from solution. The deactivation of the film by ion exchange is a secondary factor. The deactivation may be considered to shorten the column and therefore to increase the value of c_{out}/c_{in} with time. The performance of the foam therefore depends on the length of the foam, the mass transfer coefficient, the specific surface area of the foam and the fractional deactivation of the film.

It is concluded that the reactor performance could be improved further by increasing the length of the foam and increasing the specific surface area of the active structure; this could be achieved using materials such as Ni Tysar^R, Ni wool or a bed of fine Ni particles.

Our experiments confirm ESIX process is capable of effective scale-up and that it could contribute to the clean up of streams containing radioactive cesium isotopes.

1. Introduction

The experimental program has been designed to extend the work carried out at Pacific Northwest National Laboratory on Electrically Switched Ion Exchange (ESIX) for the removal of Cs^+ from a variety of waste streams. The objective was to investigate the process using a larger Ni foam within a commercial electrolytic cell.

The approach has been to convert the surface film to its fully reduced $\text{Na}_2\text{NiFe}(\text{CN})_6$ form and then to remove the Cs^+ from the feed by ion exchange without the application of a current or potential (ie. the coated foam is on open circuit). The layer is then regenerated into the Na^+ form by oxidation using a constant current. The experiments have been carried out in a commercial MP cell (manufactured by ElectroCell AB) which allows the use of a Ni Foam with the dimensions, 100 mm x 100 mm x 6.3 mm. This is of sufficient volume to permit once-through flow of the Cs^+ solutions, at least at low flow rates. The removal of the Cs^+ from the film by anodic oxidation using a constant current has also been investigated. The experiments have been carried out as a function of Cs^+ concentration, feed flow rate and the ratio of $\text{Na}^+:\text{Cs}^+$ in the feed.

The results may be fitted to a simple model that takes into account mass transfer of Cs^+ to the surface as well as loading and consequent deactivation of the film by Cs^+ . The model confirms the critical role of mass transport in the ESIX process. For once-through operation, a long contact length between foam and solution is essential and flow-by (vertical flow) operation is essential. If the process is operated in a batch recycle mode, the flow could be in either direction but operation in the vertical mode results in a higher mean linear flow velocity, hence more efficient mass transport conditions and rate of removal.

2. Modeling the Cs^+ Removal in a Foam Column – Selection of Practical Parameters

Firstly, it should be recognized that the terms “flow by” and “flow through” are only correctly applicable to experiments when current is flowing through the Ni foam; the terms describe whether the directions of solution flow and current flow are perpendicular or parallel respectively. On open circuit, it is perhaps more appropriate to use the terms vertical and cross flow, see figure 1(a).

If, initially, it is assumed that the removal of Cs^+ at the surface of the $\text{Na}_2\text{NiFe}(\text{CN})_6$ film is mass transport controlled (ie. the fastest possible rate of removal) and that the foam may be modelled as a plug flow reactor, the Cs^+ concentration at the outlet is given by

$$\frac{c_{\text{out}}}{c_{\text{in}}} = \exp\left(-\frac{k_m A_e V_e}{Q_v}\right) \quad (1)$$

irrespective of the direction of the flow. Here, c_{in} and c_{out} are the concentrations at the inlet and outlet respectively, k_m the mass transfer coefficient, A_e the specific surface area of the foam, V_e the volume of the foam and Q_v the volumetric flow rate of the solution.

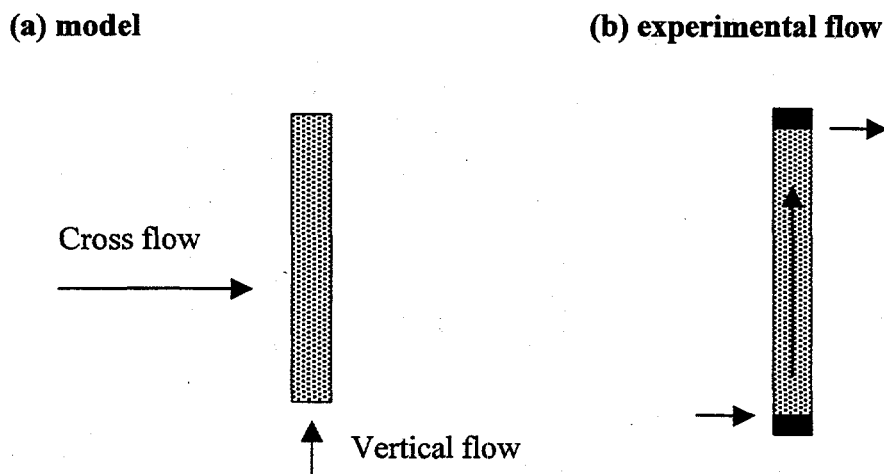


Figure 1 Comparison of (a) the ideal flow through a foam bed on open circuit with (b) the flow achieved in a commercial electrolysis cell, the MP cell, modified to contain a Ni foam with dimensions, 100 mm x 100 mm x 6.3 mm.

The foam will, however, show different performance with the two flow directions since k_m is a function of mean linear flow velocity (v) which, unlike the volumetric flow rate, depends on the direction of flow. This is illustrated in table 1 for one of the foams used in this study (80 ppi and a porosity of 80%) and a volumetric flow rate of $5 \text{ cm}^3 \text{ min}^{-1}$. The values of $k_m A_e$ were calculated using the equation

$$k_m A_e = 1.89 \times 10^{-2} v^{0.7} \quad (2)$$

taken from Pletcher et al (J. Applied Electrochem. 24 (1994) 95) table 2, although this does necessitate a long extrapolation between the rather different flow rates used in the two sets of experiments. Such calculations are very approximate but clearly show the different volumes of foam required with the two flow regimes. With vertical flow and for $c_{out}/c_{in} = 0.1$, the volume of foam is comparable to that used in this work (dimensions 100 mm x 100 mm x 6.3 mm, volume 63 cm^3) but with cross flow the foam must be a factor of seven larger. Better agreement between experiment and theory could be obtained by assuming a higher value for $k_m A_e$.

	$v/\text{cm s}^{-1}$	$k_m A_e/\text{s}^{-1}$	V_e/cm^3 for $c_{\text{out}}/c_{\text{in}} = 0.1$	
			0.1	0.01
Crosswise flow	1.04×10^{-3}	1.54×10^{-4}	1240	2480
Vertical flow	1.65×10^{-2}	1.07×10^{-3}	180	360

Table 1 Estimates of $k_m A_e$ and conversions as a function of flow direction.

A number of conclusions may be drawn:

- (i) With a reactor involving a heterogeneous reaction, the conversion of reactant can never be 100% and always depends on the total area of surface available and the mass transport regime. Hence, the term "column break through" implies a decision as to an acceptable level of Cs^+ at the outlet.
- (ii) The specific surface area of the Ni foams are high compared to traditional electrode materials but remain low compared to commercial ion exchange resins.
- (iii) The table shows that the size of the foam required depends strongly on the conversion sought - 99% removal of the Cs^+ requires a foam volume twice that for 90% removal.
- (iv) Also the conversion is independent of the Cs^+ inlet concentration. Hence, operation at very low Cs^+ concentrations will be the same unless other chemical factors intercede. On the other hand, with low Cs^+ concentrations, the $c_{\text{out}}/c_{\text{in}}$ chosen has to reflect the lowest detection limit of the Cs^+ analysis; with 0.2 ppm and the analytical method used in this work, the lowest limit of $c_{\text{out}}/c_{\text{in}}$ is ≈ 0.1 .
- (v) The plug flow reactor equation, equation (1) above, may be rewritten

$$\frac{c_{\text{out}}}{c_{\text{in}}} = \exp - \frac{k_m A_e L}{v} \quad (3)$$

where L is the length of the foam and v the mean linear flow velocity of the solution. It can be seen that for single pass operation, the foam should be as long as possible in order to give the lowest outlet concentration.

- (vi) For a particular cell geometry and size, the performance will be relatively insensitive to the feed flow rate because $k_m A_e/v$ is proportional only to $v^{-0.3}$.

The model so far only recognizes mass transport control. For Cs^+ exchange at a $\text{Na}_2\text{NiFe}(\text{CN})_6$ film covered Ni foam, a more complete model needs to recognize that, as the layer is converted to $\text{Cs}_2\text{NiFe}(\text{CN})_6$, effectively the active surface area will decrease.

The extent of removal of Cs^+ will get worse with time. The period of acceptable performance will depend on the relative values of the foam length and the critical length to achieve the required removal.

The next level of model would calculate the fraction, θ , of the sodium ions within the film exchanged for cesium from the volume of solution treated and the previous performance of the reactor. The instantaneous fractional removal at that time could then be calculated from the equation

$$\frac{c_{\text{out}}}{c_{\text{in}}} = \exp - \theta \frac{k_m A_e V_e}{Q_v} \quad (4)$$

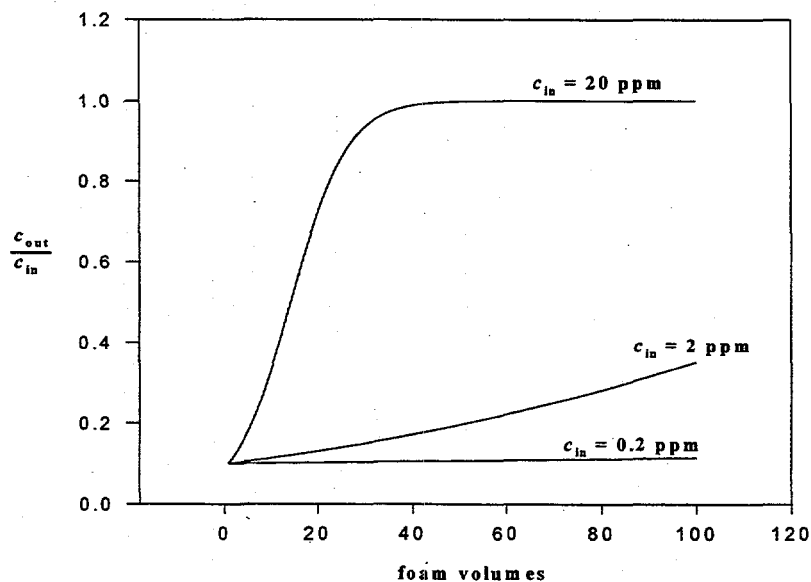


Figure 2 Plots of conversion vs volume of feed, showing the influence of Cs^+ concentration on reactor performance using the model and one set of experimental conditions (see text).

This function may be used to compute a plot of $c_{\text{out}}/c_{\text{in}}$ vs number of foam bed volumes for any inlet concentration and other experimental conditions. Figure 2 shows such theoretical plots for experimental conditions where the volume of foam is 180 cm^3 , $k_m A_e = 1.07 \times 10^{-3} \text{ s}^{-1}$, volumetric flow rate = $0.083 \text{ cm}^3 \text{ s}^{-1}$. The layer of $\text{Na}_2\text{NiFe}(\text{CN})_6$ on the foam is able to exchange 52 mg of Cs^+ . It can be seen that this model predicts no

significant change in the reactor performance during operation lasting 100 foam volumes when the inlet concentration of Cs^+ is 0.2 ppm. The value of $c_{\text{out}}/c_{\text{in}}$ is 0.1 because of the experimental parameters put into the model. In contrast, with an inlet concentration of 20 ppm, the performance is initially the same but decays rapidly because the $\text{Na}_2\text{NiFe}(\text{CN})_6$ layer is rapidly loaded with Cs^+ . The 2 ppm solution shows intermediate behavior.

The model works well because most of the exchange will occur where the solution first meets unloaded $\text{Na}_2\text{NiFe}(\text{CN})_6$ surface. Equations (3) and (4) both show that the concentration of Cs^+ drops off exponentially through the foam and hence the major part of the exchange occurs initially close to the inlet. Then as the film becomes loaded, the reaction zone will move as a front through the foam, the effective length of the foam decreasing with time. It is possible to consider three situations which depend on the relative values of the experimental bed length, L , and the critical active foam length, L_{crit} , necessary to achieve the desired extent of Cs^+ removal.

- (i) For $L < L_{\text{crit}}$, the desired level of Cs^+ removal will not be achieved even at the commencement of an experiment.
- (ii) For $L > L_{\text{crit}}$, the desired level of Cs^+ removal will be achieved for an extended period of time, the period depending mainly on the Cs^+ concentration.
- (iii) For $L \approx L_{\text{crit}}$, the desired level of Cs^+ removal may be achieved for a short period but a decay in performance will soon set in. The performance will depend strongly on the Cs^+ concentration.

The next level of modelling could take into account any kinetics associated with the insertion of Cs^+ into the $\text{Na}_2\text{NiFe}(\text{CN})_6$ layer. Studies with films on two-dimensional electrodes, however, provide no evidence that the kinetics of insertion are ever slow and this additional level of modelling has not been attempted.

The experiments in this program were all carried out in a commercial electrochemical cell, the MP cell manufactured by ElectroCell AB. This allowed the introduction of a foam with dimensions 100 mm x 100 mm x 6.3 mm, volume 63 cm³. The flow, however, is not precisely vertical flow. The flow is sketched in figure 1(b). Because of the ratio of length to width (100 mm to 6.3 mm), the reactor would be expected to behave similarly to a vertical flow reactor of the same dimensions; it is, however, not possible to quantify the deviations from ideal vertical flow. The design and fabrication of a purpose built reactor could remove this uncertainty.

3. Experimental

(a) **Film Preparation:** Porous nickel foams of porosity 60 and 80 ppi were used for all experiments. The electrode dimensions were 100 x 100 x 6.3 mm to fit in an MP flow cell. The film was cleaned initially with deionized water and the film application was done in a large beaker (2-liter) using platinum as counter-electrode. A Luggin probe was used to measure the potential at the foam electrode using Ag/AgCl reference electrode. The cell is shown in Figure 3. The method used to deposit films was a PNNL-proprietary variation of the method of Bocarsly, et al. The electrolyte for film deposition was a solution containing 0.1 M KNO_3 and 0.01 M $\text{K}_3\text{Fe}(\text{CN})_6$. A PAR 273 Potentiostat was used to control the potential at 1.0 V for 360 s. At the end of deposition, the foam was taken out of the bath and rinsed in DI water. A solution of 1 M NaNO_3 was then used with similar arrangement (Pt counter-electrode, luggin probe and Ag/AgCl reference) to run cyclic voltammetric curve. All voltammograms were done at a scan rate of 50 mV s^{-1} between -0.25 and 1.05 V vs. Ag/AgCl. The area under the oxidation and reduction waves was integrated to obtain the film loading or capacity of the film. Chronocoulometric experiments were also performed to determine the film capacity. Current decay at potentials 0.8 V and 0.2 V (vs. Ag/AgCl) for 30 s each was used to measure film capacities. The areas under the current decay curves at 0.8 and 0.2 V were integrated to calculate the film capacity. The same procedure was followed to measure the electrochemical characteristics of all the films prepared.

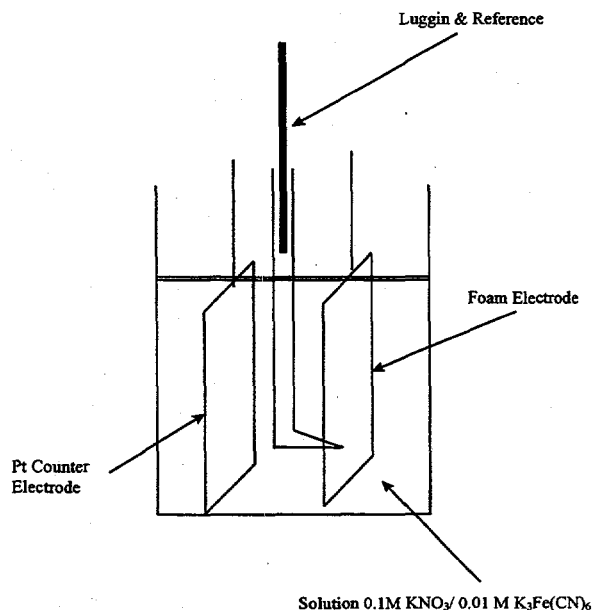


Figure 3. Beaker cell for film Deposition & CV Experiments

(b) *MP flow cell set up and cell operation:* The cell was set up in the way shown schematically in figures 4, 5 and 6. Feed solutions were prepared by dissolving CsNO_3 in DI water to the desired final Cs concentrations (20, 2 and 0.2 ppm). For studies on the effect of ionic strengths, NaNO_3 was used as the electrolyte to obtain Na^+/Cs^+ molar ratio of up to 10^5 . A Masterflex pump was used to control liquid flow through the cell at the desired rate (8 to 24 ml/min). Effluent samples were collected at different intervals for cesium analysis. Samples were analyzed by atomic absorption emission method using proper matrix for the background (see analytical procedure below).

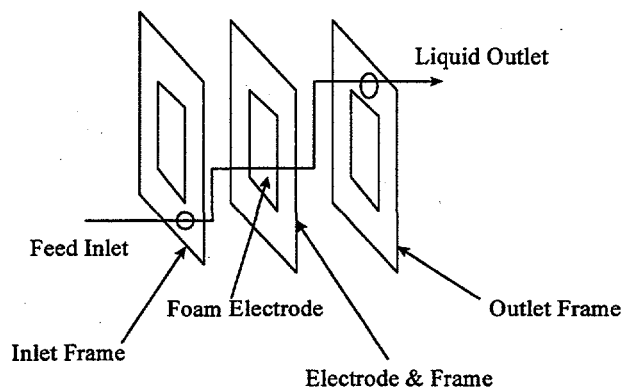
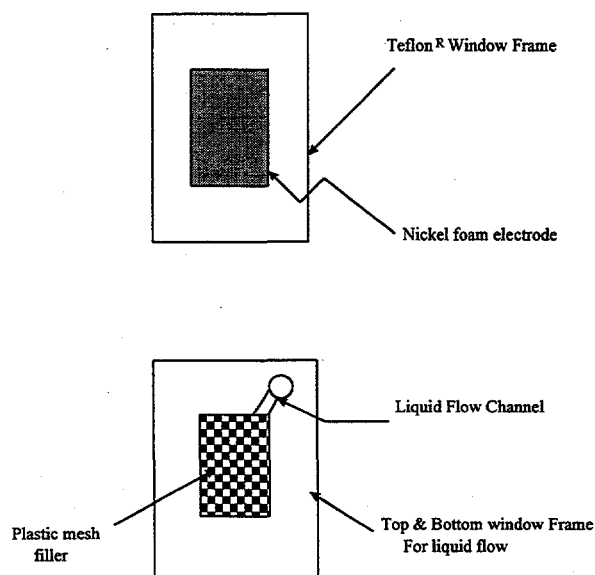


Figure 4 Electrode and frame arrangement within the cell.



Viton gaskets placed between the frames with good seals around the foam electrode.

Figure 5: Cell frames and plastic mesh spacers.

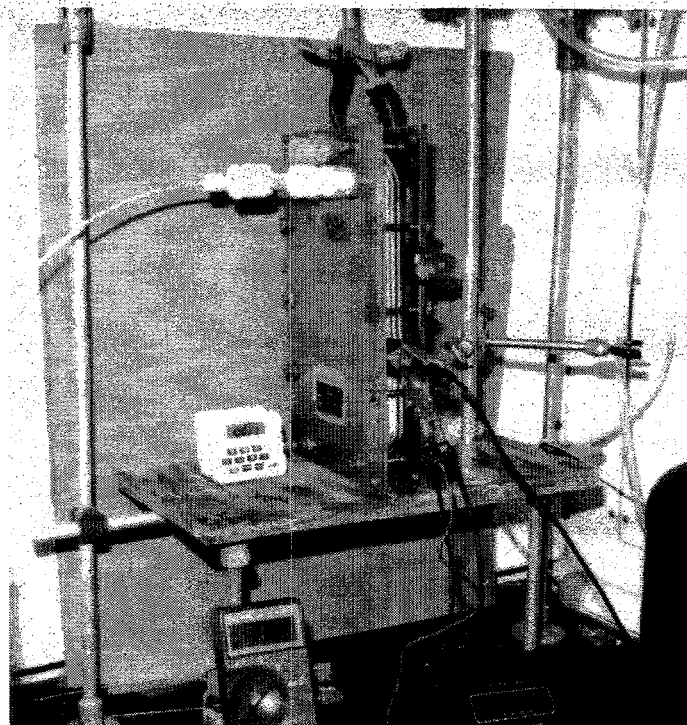


Figure 6: MP cell experimental set up.

(c) **Procedure for in-situ regeneration of the film:** A method was developed for the regeneration of film in-situ. A solution of 0.1 M NaNO_3 was passed through the cell at a flow rate while maintaining a constant current (5 mA). Passage of about 300 cm^3 of 0.1 M NaNO_3 solution for about 2 - 3 hours was sufficient to elute 70 - 75 % of the cesium exchanged on the film. The cell was completely drained and the solution to determine the amount of cesium eluted. The cell was also rinsed with DI water before further experiments using the regenerated film. During elution, very small amounts of colloidal solids were washed with the eluting solution. These were too small to analyze and may be due to the partial removal of the film or from corrosion of nickel during regeneration. This phenomenon may be attributed to the particular regeneration conditions used in these experiments since other experimental work at PNNL has shown no corrosion. Continued use of the electrode over a number of cycles shows some capacity loss. Cyclic voltammetry of films regenerated in-situ showed similar characteristics to the original film.

(d) **Atomic Absorption Emission Analytical Procedure for Cs^+ :** Cesium analysis was performed using the atomic absorption emission method. Using sodium or potassium salts in the matrix increases the sensitivity for cesium detection by emission. All standards for analysis were therefore made in 0.1 or 1 M NaNO_3 depending on the matrix used in the MP cell flow experiments. Standards (0.1 to 1 ppm Cs) were prepared in 0.1 M NaNO_3 matrix. An example of the calibration curve for the standards is given in

Figure 7. Acetylene/air (ratio of 2:4) was used for the flame and wavelength of 852.1nm for cesium detection. A red filter to absorb any radiation below 650nm was also used throughout the analysis. A Perkin-Elmer 3110 was used for analysis. Samples collected from different experiments were diluted to appropriate concentration to make up the final mixture to 0.1 M NaNO₃. The concentration of cesium was then obtained using the calibration curve for cesium from the emission measured for the sample. The lower limit of detection for cesium under these conditions was < 20 ppb. A background solution of 0.1 M NaNO₃ was used to zero the emission background for both the sample analysis and standard calibration.

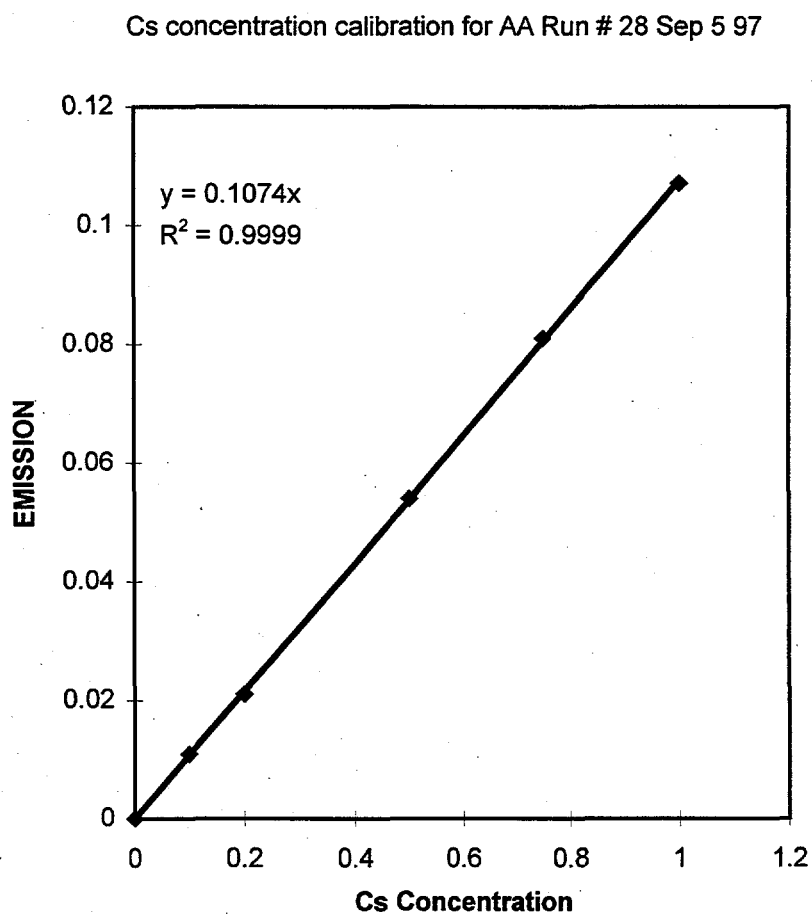


Figure 7: Calibration curve for Emission Spectroscopy

4. Results

4.1 Characterization of the Coated Ni Foams

The 60 and 80 ppi Ni foams were coated with a film of $\text{Na}_2\text{NiFe}(\text{CN})_6$ using a standard procedure similar to that developed in the laboratories of PNNL. The only difference was that the Ni foam was acid washed prior to the film formation. This increased the charge associated with oxidation/reduction of the film and the ion exchange capacity of the film. All freshly prepared coated electrodes (in the Na^+ form) were first characterized using both cyclic voltammetry and a double potential step method. The results were very reproducible and only typical data are reported here.

Figure 8 shows a typical cyclic voltammogram of the $\text{Na}_2\text{NiFe}(\text{CN})_6$ film on 60 ppi Ni foam in 1M NaNO_3 recorded at 50 mV s^{-1} . Well defined oxidation and reduction peaks are clearly observed although both peaks are drawn out compared to those reported

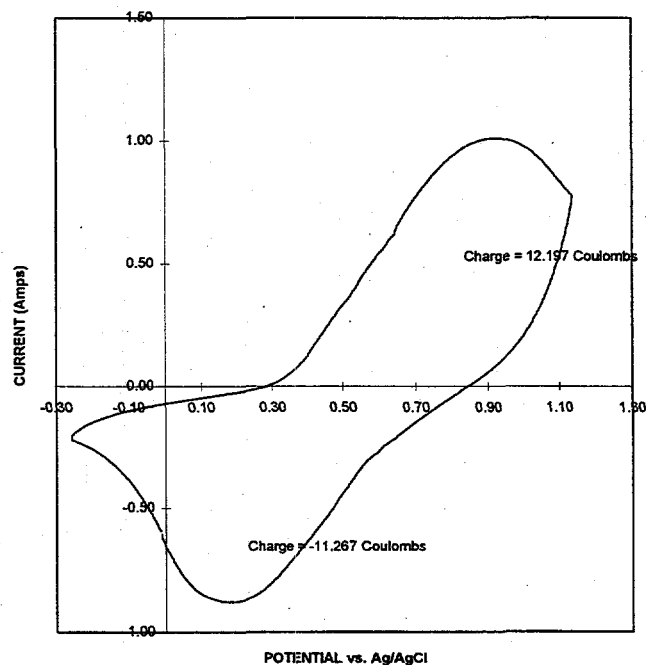


Figure 8: Typical cyclic voltammogram of the $\text{Na}_2\text{NiFe}(\text{CN})_6$ film on 60 ppi Ni foam in 1M NaNO_3 recorded at 50 mV s^{-1}

previously on two dimensional electrodes. This is to be expected, however, in an experiment where the currents approach 1 A; it is inevitable that there is significant uncorrected IR drop despite the use of a three electrode cell. The charges associated with the oxidation and reduction processes are ≈ 12.2 C and ≈ 11.3 C respectively. This is not a significant difference because over the wider potential range employed, there may be contribution from other reactions, for example, oxygen evolution. The average charge corresponds to a charge density of 2 mC cm^{-2} (electrode volume 63.5 cm^3 , specific surface area $60 \text{ cm}^2 \text{ cm}^{-3}$) or a capacity density of $2 \times 10^{-8} \text{ moles cm}^{-2}$. This is a similar charge density to those obtained on two-dimensional electrodes. It was concluded that the coating procedure for the foams was satisfactory.

Figure 9 reports the analogous chronoamperometric response when the same film was subjected to potential steps to + 800 mV and then 0 mV in 1 M NaNO_3 . Again, the precise form of the response should not be interpreted because of uncorrected IR drop. It is, however, confirmed that the rate of Cs^+ loading and discharge are both high, with currents above 1 A being achieved. It can also be seen that the charge balance is again good and that the charge cycled in the potential steps is similar to those in the cyclic voltammetry.

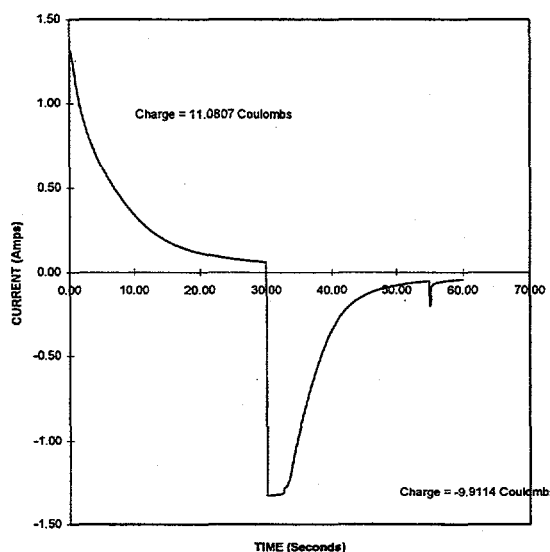


Figure 9: Chronoamperometric response

These experiments with the foams confirm that the movement of ions into and out of the film is rapid and there is no reason to invoke any control by the kinetics of ion movement in the film. Table 2 summarizes some data for the films showing the advantage of acid washing the Ni foam before the $\text{Na}_2\text{NiFe}(\text{CN})_6$ film is formed.

In many experiments, cyclic voltammograms and potential step experiments were repeated during and/or after the use of the films for Cs^+ removal. No significant changes to the responses were observed although it should be noted that the fractional exchange of Na^+ by Cs^+ within the films was generally rather low in these experiments. In no experiments was the exchange driven near to completion before its voltammetry was examined.

Grade Ni foam	$A_e/\text{cm}^2 \text{ cm}^{-3}$	Water washed		Acid washed	
		Charge/C	Capacity/mg Cs^+	Charge/C	Capacity/mg Cs^+
60 ppi	60	5.4	7.4	13.0	17.8
80 ppi	75	7.0	9.6	12.1	16.6

Table 2 Charges and capacities of $\text{Na}_2\text{NiFe}(\text{CN})_6$ films on Ni foams after two different pretreatments. Specific surface areas taken from *J. Applied Electrochem.* 19 (1989) 43.

4.2 The Removal of Cs^+ by $\text{Na}_2\text{NiFe}(\text{CN})_6$ coated Ni Foams on Open Circuit

Figures 10 and 11 report the experimental results from an experiment carried out with a 60 ppi Ni foam (dimensions 100 mm x 100 mm x 6.3 mm, volume 63 cm^3) coated with a $\text{Na}_2\text{NiFe}(\text{CN})_6$ layer with a Cs^+ capacity equivalent to 17.9 mg. The inlet concentration was 2.4 ppm Cs^+ and the flow rate 0.1 $\text{cm}^3 \text{ s}^{-1}$. Figure 10 shows the variation of $c_{\text{out}}/c_{\text{in}}$ with the volume of the inlet stream while figure 11 shows the consequent build up of Cs^+ cation in the film.

Model calculations would suggest that in these experiments, the maximum removal of Cs^+ with the fresh $\text{Na}_2\text{NiFe}(\text{CN})_6$ layer would be $\approx 90\%$. The MP cell dimensions determined the foam size used. It would have been advantageous to have been able to vary the foam length since the experiments are all carried out in the situation where $L \approx L_{\text{crit}}$ and the data would look markedly different if, for example, the foam had been twice as long, ie. 200 mm, without changing other parameters.

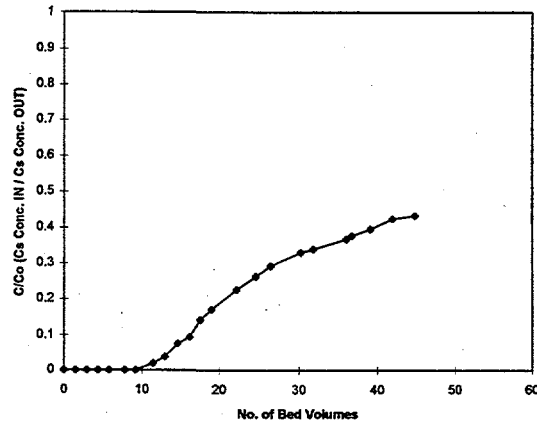


Figure 10: Cesium Concentration as a function of volume passed; Cs concentration 2.4ppm; film capacity 17.9 mg of Cs.

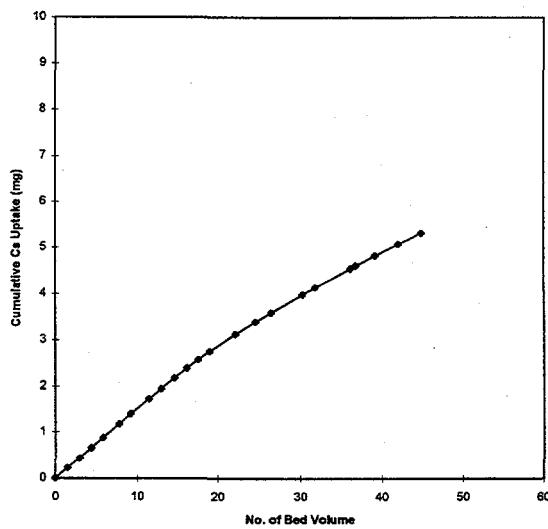


Figure 11: Cesium Uptake as a function of volume passed; Cs concentration 2.4ppm; film capacity 17.9 mg of Cs.

The experimental data shows that initially the foam does rather better than predicted in the model calculations (although because of uncertainty in the lowest detection limit for the analysis, we would caution interpretation of $c_{out}/c_{in} = 0$). After 16 bed volumes of solution, the value of $c_{out}/c_{in} = 0.1$; at this point 13% of the bed has been transformed to the Cs^+ form and some decay in performance might indeed be expected. The slope of the plot of cumulative Cs^+ uptake versus solution volume begins to decrease but cumulative Cs^+ uptake continues. By the termination of the experiment after a volume of solution equivalent to 45 bed volumes, the cumulative Cs^+ uptake has reached 29% and there is a significant decay in the performance of the foam. The value of c_{out}/c_{in} has increased to ≈ 0.4 . We regard this as a reasonable fit with the theory (see section 2) and we believe that the performance of the foam is largely determined by mass transfer characteristics. The only approaches to significantly improving the performance would be to increase the bed length or its specific surface area.

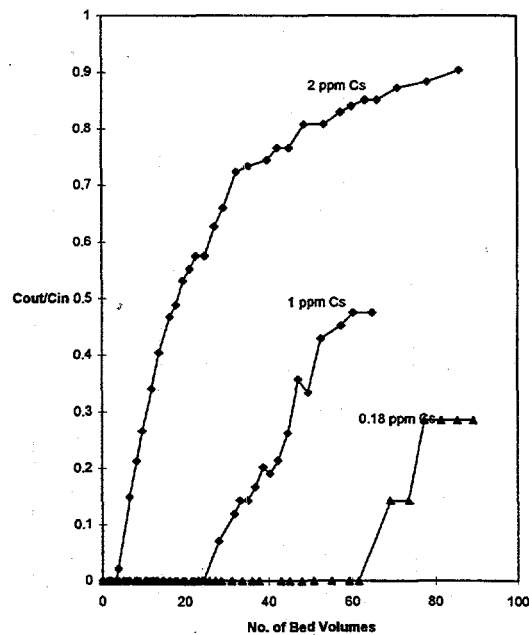


Figure 12: Cesium Concentration as a function of volume passed; Cs concentrations 2, 1, 0.18ppm

Figure 12 shows plots of c_{out}/c_{in} versus volume of Cs^+ solution for three Cs^+ concentrations while table 3 summarizes the data for four concentrations. All these experiments were carried out using foams (dimensions 100 mm x 100 mm x 6.3 mm, volume 63 cm³) with similar loadings of $Na_2NiFe(CN)_6$ (equivalent to 12 – 17 mg Cs^+) as determined voltammetrically. Again a value of $c_{out}/c_{in} = 0.1$ was chosen as the definition of “break through” and values of $c_{out}/c_{in} = 0$ should be thought of as the detection limit for the Cs^+ . In all cases, break through occurred when approximately 10 % of the cations in the layer had been exchanged and this again results from the fact the foam length is only just sufficient initially to achieve $c_{out}/c_{in} = 0.1$. The foam continues to exchange Cs^+ after break through but the observed c_{out}/c_{in} increases rapidly; typically the exchange reached 20 – 30% before experiment were discontinued. It can be seen that in this situation, the performance is very dependent on Cs^+ concentration and the foam performance appears

C_{in}/ppm	Bed volumes to $c_{out}/c_{in} = 0.1$	Fractional loading of layer by Cs^+ at $c_{out}/c_{in} = 0.1$
2.0	6	0.08
1.35	17	0.10
1.03	27	0.12
0.18	65	0.06

Table 3 Performance of the 60 ppi Ni foam (dimensions 100 mm x 100 mm x 6.3 mm, volume 63 cm³) with loadings of $Na_2NiFe(CN)_6$ (equivalent to 12 – 17 mg Cs^+). Flow rates 8 – 12 foam volumes/hour.

ppi	Foam Cs capacity/mg	Bed volumes to $c_{out}/c_{in} = 0.1$	Fractional loading of layer by Cs^+ at $c_{out}/c_{in} = 0.1$
60	11.6	90	0.09
	13.8	110	0.10
	13.8	100	0.12
80	4.4	38	0.09
	16.7	100	0.07
	16.7	80	0.09
	16.7	120	0.10
	16.7	80	0.10
	16.7	80	0.09

Table 4 Performance of the Ni foam (dimensions 100 mm x 100 mm x 6.3 mm, volume 63 cm³). Flow rates 8 – 12 foam volumes/hour.

to improve substantially as the concentration is decreased. The general form of the data resembles that predicted by the model and shown in figure 2.

A large number of experiments have been carried out with a Cs^+ concentration of 0.2 ppm and the data are summarized in table 4. Generally, the experiments have been carried out in similar conditions and are reported here to emphasize the reproducibility of the experimental data. It is, however, clear that a large change in loading by $Na_2NiFe(CN)_6$ does influence the performance; in the experiment with a thin film equivalent to only 4.4 mg of Cs^+ break through occurs at a much lower solution volume although at a similar value of fractional ion exchange.

The data does not distinguish the performance of 60 ppi and 80 ppi foam. This is not surprising since the specific surface areas are not markedly different, 60 and 75 cm² cm⁻³. It is to be expected that a large increase in the specific surface area would improve the performance and materials such as Ni Tysar^R, Ni wools and beds of small Ni particles would be worth investigating. Also, experiments with the solution flow rate varied between 8 and 23 foam volumes/hour showed no significant trends. It was predicted in

the discussion of the model that a large change in flow rate would be necessary to cause marked changes to the data.

The final parameter investigated was the concentration of Na^+ in the inlet stream. Data from an experiment where the inlet stream contained 0.2 ppm Cs^+ and 200 ppm Na^+ are reported in figures 13 and 14. In figure 13, it can be seen that $c_{\text{out}}/c_{\text{in}}$ becomes > 0.1 after ≈ 85 foam volumes and this falls within the range found for solutions containing only Cs^+ (see table 4). Similarly, figure 14 confirms that the ion exchange of Na^+ by Cs^+ within the $\text{Na}_2\text{NiFe}(\text{CN})_6$ layer does not seem to have been changed by the presence of Na^+ in solution. In a further experiment where the Na^+ concentration in the inlet stream was even higher, 20000 ppm, the experimental results were unexpected. The plot of $c_{\text{out}}/c_{\text{in}}$ vs solution volume is shown in figure 15. It can be seen that the coated foam initially performs very badly with $c_{\text{out}}/c_{\text{in}} > 0.3$. The rate of removal of Cs^+ then improves before a perhaps normal fall off in performance is observed after 80 – 100 bed volumes. This result was reproduced in a second experiment but we presently have no explanation. Such behavior is not predicted by the model (which would not suggest any influence of Na^+ concentration) and is neither a mass transport nor a ion exchange capacity effect. It could, for example, arise through the high level of Na^+ ion effecting the structure/swelling of the $\text{Na}_2\text{NiFe}(\text{CN})_6$ layer.

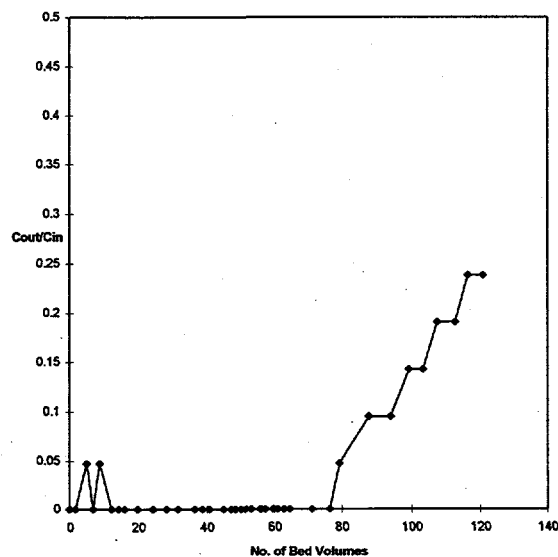


Figure 13: Cesium Concentration as a function of volume passed; Cs concentration 0.2ppm, Sodium concentration 200ppm

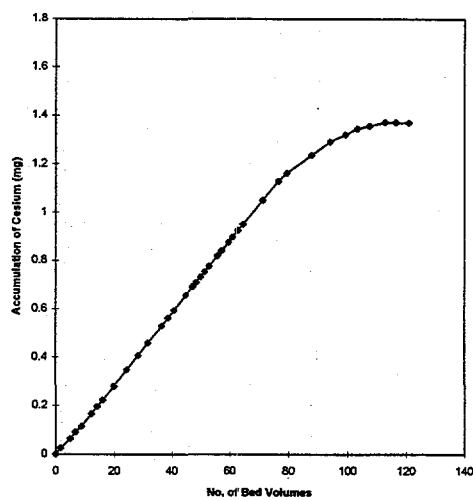


Figure 14: Cesium Uptake as a function of volume passed; Cs concentration 0.2ppm, Sodium concentration 200ppm

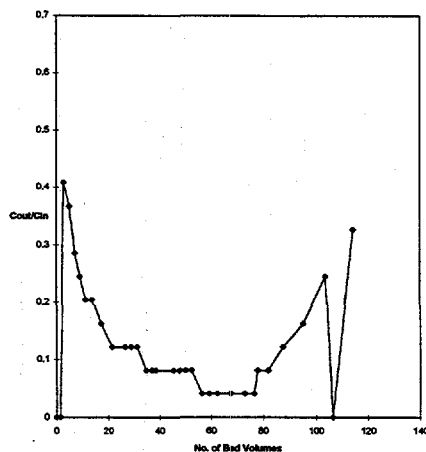


Figure 15: Cesium Concentration as a function of volume passed; Cs concentration 0.2ppm, Sodium concentration 20,000ppm

4.3 The Recovery of Cs⁺ from the Na_{2-x}Cs_xNiFe(CN)₆ Layer

The removal of the Cs⁺ from the film on the Ni foam by anodic oxidation has been studied. The electrode reaction



will clearly lead to removal of a cation from the film and under some circumstances it will be Cs⁺ which will be ejected. Since the thermodynamics of binding of the Cs⁺ within the layer are more favorable than those for Na⁺, removal of the Cs⁺ will only occur where, locally, within the layer, the fraction of Cs⁺ is high. As noted earlier, this will be the case close to the inlet to the foam and through the foam as more complete exchange is carried out during loading. During removal of the Cs⁺, a further problem could be envisaged – the Cs⁺ could exchange back on to the film further down the foam towards the exit.

Four experiments were carried out where a Ni foam (dimensions 100 mm x 100 mm x 6.3 mm, volume 63 cm³) with a Na₂NiFe(CN)₆ layer (Cs⁺ capacity equivalent to 10 – 12 mg) was loaded with to an extent of 15 – 20 % with Cs⁺ using a solution containing 0.2 ppm Cs⁺. The Cs⁺ loaded foam was then oxidized using a constant current of 5 mA while passing a solution of 0.1 M Na NO₃ (300 cm³) through the foam with a flow rate of 1 cm³ s⁻¹. The eluent was ≈ 3 ppm in Cs⁺ and the total recoveries of Cs⁺ were between 60 and 80 %.

These experiments were all carried out at with a current of 5 mA, a very low current density. The voltammetric response would suggest that it would be possible to discharge most of the Cs⁺ at a much higher rate, thus giving a higher Cs⁺ concentration in the eluent and a higher concentration factor. The low current was employed in these preliminary experiments to avoid possible competing electrode reactions such as oxygen evolution.

5. Conclusions

It has been confirmed that the selective removal of Cs⁺ from aqueous effluent is possible using a Ni foam coated with a Na₂NiFe(CN)₆ layer. The coated Ni foams appear to have very similar characteristics and voltammetric properties to a Na₂NiFe(CN)₆ films on small, two dimensional electrodes.

A reactor built by modifying an MP cell to include a Ni foam (dimensions 100 mm x 100 mm x 6.3 mm, volume 63 cm³) has been tested. It is shown that the performance of the foam, operated on open circuit, depends strongly on the Cs⁺ concentration. The film loading, solution flow rate and grade of Ni foam have also been

varied but influence the performance less strongly. Preliminary experiments also confirm that the Cs^+ may be removed from the film by anodic oxidation.

The behavior of the reactor can be understood in terms of a model which includes the role of mass transfer and the deactivation of the $\text{Na}_2\text{NiFe}(\text{CN})_6$ film as the Na^+ cations within the layer are replaced by Cs^+ . The model stresses the role of mass transport in determining the minimum path length, L_{crit} , of the solution through the foam necessary to make possible the desired extent of removal of Cs^+ from solution. The deactivation of the film by ion exchange is a secondary factor. The deactivation may be considered to shorten the column and therefore to increase the value of $c_{\text{out}}/c_{\text{in}}$ with time. The performance of the foam therefore depends on the length of the foam, the mass transfer coefficient, the specific surface area of the foam and the fractional deactivation of the film.

All the experiments in this report were carried out in a reactor where the length of the foam was only just sufficient to permit an outlet concentration as low as $0.1c_{\text{in}}$ (ie. $L \approx L_{\text{crit}}$). Hence, the performance decayed rather rapidly as the layer deactivated; for example, with a solution containing 0.2 ppm Cs^+ , $c_{\text{out}}/c_{\text{in}} > 0.1$ after ≈ 100 foam volumes when only 10% of the bed had deactivated. There would be a substantial advantage in doubling the foam length when it would be expected that $c_{\text{out}}/c_{\text{in}} = 0.1$ would not be reached until ≈ 1500 foam volumes when $> 50\%$ of the bed would be deactivated. There is also an advantage in investigating Ni materials with a higher specific surface area; possible materials include Ni Tysar^R, Ni wool of a bed of fine Ni particles.

Distribution

No. of
Copies

No. of
Copies

OFFSITE

Dr. Moses Attrep, Jr.
Los Alamos National Laboratory
P.O. Box 1663, MS J514
Los Alamos, NM 87545

Ms. Debra A. Bostick
Oak Ridge National Laboratory
P.O. Box 2008
Oak Ridge, TN 37831-6201

Professor Daryle Busch
University of Kansas
Department of Chemistry
Lawrence, KS 66045

Professor Greg Choppin
Florida State University
Department of Chemistry
600 West College Avenue
Tallahassee, FL 32306

Ms. Julie E. Connor
U.S. Department of Energy
Idaho Operations Office
765 Lindsay Blvd., Mailstop 1225
Idaho Falls, ID 83401

Dr. J. David Genders
The Electrosynthesis Company, Inc.
72 Ward Road
Lancaster, NY 14086-9779

Dr. Dirk Gombert
Lockheed Martin Idaho Technologies
P.O. Box 1625, Mail Stop 3875
Idaho Falls, ID 83415

Dr. Ram Gopal
The Electrosynthesis Company, Inc.
72 Ward Road
Lancaster, NY 14086-9779

Mr. Kurt Gerdes
U.S. Department of Energy
Program Manager
Efficient Separations and Processing
Office of Science and Technology
EM-53 CL
19901 Germantown Road
Germantown, MD 20874

Dr. Jerry L. Harness
U.S. Department of Energy
Oak Ridge Operations Office
P.O. Box 2001, 3-MAIN
Oak Ridge, TN 37831

Prof. Dennis Kelsh
Gonzaga University
Department of Chemistry
E. 505 Boone Ave.
Spokane, WA 99258-0001

Dr. John H. Kolts
U.S. Department of Energy
Idaho Operations Office
765 Lindsay Blvd., Mailstop 1147
Idaho Falls, ID 83401

Prof. KNona Liddell
Washington State University
Department of Chemical Engineering
Pullman, WA 99164-2710

**No. of
Copies**

Mr. John Mathur
U.S. Department of Energy
Office of Science and Technology
EM-53 CL
19901 Germantown Road
Germantown, MD 20874

Mr. Phil McGinnis
Martin Marietta Energy Systems
4500-N, MS-6273
P.O. Box 2008
Oak Ridge, TN 37831

Mr. Jim McGlynn
Science Applications International Corp.
555 Quince Orchard Road, Suite 500
Gaithersburg, MD 20878

Mr. Bruce Monzyk
Battelle Memorial Institute
505 King Avenue
Columbus, Ohio 43201-2693

Dr. Don Orth
124 Vivion Drive
Aiken, SC 29803

Dr. James Phelan
Sandia National Laboratories
P.O. Box 5800, Mail Stop 0719
Albuquerque, NM 87185-0719

Dr. Martin Steindler
Argonne National Laboratory
9700 South Cass Avenue
Argonne, IL 60439

Dr. Dee Stevenson
3367 E. Bernada Drive
Salt Lake City, UT 84124

**No. of
Copies**

Dr. John Swanson
1318 Cottonwood Dr.
Richland, WA 99352

Dr. Ian R. Tasker
Waste Policy Institute
Quince Diamond Executive Center
555 Quince Orchard Road
Gaithersburg, MD 20878-1437

Dr. Major Thompson
Savannah River Technology Center
P.O. Box 616
Aiken, SC 29802

Dr. Terry Todd
Lockheed Martin Idaho Technologies
P.O. Box 1625
Idaho Falls, ID 83415-5213

Dr. Paul Usinowicz
Battelle Memorial Institute
505 King Avenue
Columbus, Ohio 43201-2693

Dr. Jack Watson
Oak Ridge National Laboratory
P.O. Box 2008
Oak Ridge, TN 37831-6149

Dr. J. A. Wright
U.S. Department of Energy
Savannah River Operations Office
P.O. Box A
Aiken, SC 29808

Dr. Ray Wymer
188A Outer Drive
Oak Ridge, TN 37831

**No. of
Copies**

**No. of
Copies**

ONSITE

34 Pacific Northwest National Laboratory

5 DOE Richland Operations Office

T. L. Aldridge K8-50
J. P. Hanson K8-50
C. S. Louie B4-55
R. A. Pressentin K8-50
B. M. Mauss K8-50

Duke Engineering & Services, Inc.

D. R. Precechtal X3-85

Lockheed Martin Hanford Company

J. N. Appel H6-37

5 Numatec Hanford Company

D. B. Bechtold T6-07
J. Bourges T6-07
D. L. Herting T6-07
J. R. Jewett T6-07
R. A. Kirkbride H5-27

SGN Eurisys Services Corporation

R. K. Biyani B4-51

E. G. Baker K2-12
W. F. Bonner K9-14
T. M. Brouns K9-91
G. N. Brown P7-25
J. L. Buelt K2-14
R. T. Hallen K2-12
W. L. Kuhn K8-93
D. E. Kurath P7-28
J. P. LaFemina P7-27
W. E. Lawrence P7-41
M. A. Lilga (10) P8-38
N. J. Lombardo K9-04
R. J. Orth K3-75
M. E. Peterson K2-20
S. D. Rassat P7-41
S. C. Slate K1-50
T. L. Stewart K9-69
J. P. H. Sukamto K8-93
Information Release (7)